# Diurnal tides from the troposphere to the lower mesosphere as deduced from TIMED/SABER satellite data and six global reanalysis data sets

T. Sakazaki,[1] M. Fujiwara,[1] X. Zhang,[2] M. E. Hagan,[3] and J. M. Forbes[2]

Received 7 November 2011; revised 17 April 2012; accepted 18 April 2012; published 6 July 2012.

[1] We compare and examine diurnal temperature tides including their migrating component (DW1) from the troposphere to the lower mesosphere, using data from Thermosphere-Ionosphere-Mesosphere-Energetics and Dynamics/Sounding of the Atmosphere using Broadband Emission Radiometry (TIMED/SABER) and from six different reanalysis data sets: (1) the Modern Era Retrospective analysis for Research and Applications (MERRA), (2) the European Centre for Medium-range Weather Forecasts (ECMWF) reanalysis (ERA-Interim) (3) the National Centers for Environmental Prediction (NCEP) Climate Forecast System Reanalysis (CFSR), (4) the Japanese 25-year reanalysis by Japanese Meteorological Agency (JMA) and the Central Research Institute of Electric Power Industry (CRIEPI) (JRA25), (5) the NCEP/National Center for Atmospheric Research reanalysis (NCEP1), and (6) the NCEP and Department of Energy (DOE) Atmospheric Model Intercomparison Project (AMIP-II) reanalysis data (NCEP2). The horizontal and vertical structures of the diurnal tides in SABER and reanalyses reasonably agree, although the amplitudes are up to 30–50% smaller in the reanalyses than in the SABER in the upper stratosphere to lower mesosphere. Of all tidal components, the DW1 is dominant while a clear eastward propagating zonal wave number 3 component (DE3) is observed at midlatitudes of the Southern Hemisphere in winter. Among the six reanalyses, MERRA, ERA-Interim and CFSR are better at reproducing realistic diurnal tides. It is found that the diurnal tides extracted from SABER data in the winter-hemisphere stratosphere suffer from sampling issues that are caused by short-term variations of the background temperature. In addition, the GSWM underestimates the amplitude in the midlatitude upper stratosphere by about 50%.

**Citation:** Sakazaki, T., M. Fujiwara, X. Zhang, M. E. Hagan, and J. M. Forbes (2012), Diurnal tides from the troposphere to the lower mesosphere as deduced from TIMED/SABER satellite data and six global reanalysis data sets, *J. Geophys. Res.*, *117*, D13108, doi:10.1029/2011JD017117.

## 1. Introduction

[2] Atmospheric thermal tides are global-scale waves with periods that are harmonics of a solar day, which are mainly excited in the lower and middle atmosphere by the diurnally varying solar radiative heating absorbed by tropospheric water vapor and latent heat release in the troposphere, and the radiative heating absorbed by stratospheric ozone, respectively [*Chapman and Lindzen*, 1970]. Tides are classified by the time frequency (diurnal, semidiurnal) and the zonal wave number. In the present study, we focus on the diurnal component (i.e., diurnal tides) including its migrating component (Sun-synchronous westward propagating wave number 1 diurnal component; hereafter referred to as DW1). Since the air density decreases with increasing altitude, tidal amplitudes increase as they propagate upward, maximizing in the mesosphere and lower-thermosphere (the MLT) region for diurnal tides. Thus, many previous tidal studies focused on the MLT region using satellite temperature/wind measurements [e.g., *Forbes and Wu*, 2006; *Huang et al.*, 2006; *Wu et al.*, 2008; *Xu et al.*, 2009; *Zhang et al.*, 2006, 2010a, 2010b], ground-based wind measurements (meteor radars, lidars) [e.g., *Vincent et al.*, 1988; *Liu et al.*, 2007; *Lu et al.*, 2011], and numerical simulations [e.g., *Hagan et al.*, 1995; *Mclandress*, 1997; *Chang et al.*, 2008] (see *Ward et al.* [2010] for the comparison between observations and simulations).

[3] On the other hand, fewer studies focused on tides in the troposphere and the stratosphere, partly because the amplitudes are relatively small and partly because there have been only a few observations which can resolve diurnal

[1]Graduate School of Environmental Science, Hokkaido University, Sapporo, Japan.
[2]Department of Aerospace Engineering Sciences, University of Colorado Boulder, Boulder, Colorado, USA.
[3]High Altitude Observatory, National Center for Atmospheric Research, Boulder, Colorado, USA.

Corresponding author: T. Sakazaki, Graduate School of Environmental Science, Hokkaido University, N10 W5, Sapporo 060-0810, Japan. (zaki@ees.hokudai.ac.jp)


0148-0227/12/2011JD017117

**Table 1.** Description of Six Reanalysis Data Sets

| Data Set | Output Resolution[a] | Output Top | Model Resolution[b] | Model Top |
|---|---|---|---|---|
| MERRA[c] | 1.25° × 1.25°, L42, 3 hr | 0.1 hPa | 1/2° × 2/3°, L60 | 0.01 hPa |
| ERA-Interim[d] | 1.5° × 1.5°, L37, 6 hr | 1 hPa | T255, L60 | 0.1 hPa |
| CFSR[e] | 0.5° × 0.5°, L37, 6 hr | 1 hPa | T382, L64 | 0.266 hPa |
| JRA25[f] | 1.25° × 1.25°, L23, 6 hr | 0.4 hPa | T106, L40 | 0.4 hPa |
| NCEP1[g] | 2.5° × 2.5°, L17, 6 hr | 10 hPa | T62, L28 | 3 hPa |
| NCEP2[h] | 2.5° × 2.5°, L17, 6 hr | 10 hPa | T62, L28 | 3 hPa |

[a]The horizontal grids in longitude × latitude, number of vertical grids, and temporal resolution for the data sets used in this study.
[b]T means the truncation horizontal wave number, and Tn corresponds to ∼ (120/*n*)° grids. The horizontal resolution for ERA-Interim is $T_L255$ with N128 reduced Gaussian grids, which corresponds to ∼79 km globally. L means the number of vertical levels.
[c]See http://gmao.gsfc.nasa.gov/research/merra/intro.php.
[d]See http://www.ecmwf.int/research/era/do/get/era-interim.
[e]See http://cfs.ncep.noaa.gov/cfsr/.
[f]See http://jra.kishou.go.jp/JRA-25/index_en.html.
[g]See http://www.esrl.noaa.gov/psd/data/gridded/data.ncep.reanalysis.derived.html.
[h]See http://www.cpc.ncep.noaa.gov/products/wesley/reanalysis2/.

variations in this altitude region. However, the tidal variability in the lower atmosphere greatly impacts the tides in the MLT region [e.g., *Forbes et al.*, 2006], since it is in the lower and middle atmosphere that tides are principally excited.

[4] Early tidal studies from the troposphere to the stratosphere mostly used in-situ observations such as radiosonde soundings [*Wallace and Hartranft*, 1969; *Wallace and Tadd*, 1974; *Tsuda et al.*, 1994; *Alexander and Tsuda*, 2008], meteorological rocket soundings [e.g., *Reed et al.*, 1969], and atmospheric radars [*Riggin et al.*, 2002; *Williams and Avery*, 1996b]. These studies were mostly done in the tropics to examine the vertical profiles of tides. However, from these single-point observations, it was impossible to estimate the horizontal scale of the observed diurnal variations. That is, it is unknown whether the observed results are caused by tides or by any other local phenomena.

[5] Global tidal studies were made possible by satellite observations such as the Nimbus-7 Limb Infrared Monitor of the Stratosphere (LIMS) [*Hitchman and Leovy*, 1985; *Lieberman*, 1991] and the Upper Atmosphere Research Satellite (UARS) Microwave Limb Sounder (MLS) [*Wu et al.*, 1998], and by space shuttle observations such as the Cryogenic Infrared Spectrometers and Telescopes for the Atmosphere (CRISTA) [*Ward et al.*, 1999]. Within the last few years, tidal temperature structures from the troposphere to the stratosphere have been examined in more details using longer-term data sets from the Thermosphere-Ionosphere-Mesosphere-Energetics and Dynamics/Sounding of the Atmosphere using Broadband Emission Radiometry (TIMED/SABER) (above 20 km in altitude) [*Mukhatrov et al.*, 2009; *Huang et al.*, 2010], and from the GPS radio occultation measurements (GPS-RO) made from the CHAllenging Minisatellite Payload (CHAMP) satellite and the Constellation Observing System for Meteorology, Ionosphere, and Climate (COSMIC) satellites (between 5 km and 35 km in altitude) [*Zeng et al.*, 2008; *Pirscher et al.*, 2010; *Xie et al.*, 2010]. These studies mainly focused on the DW1 and revealed its the basic latitudinal–vertical structure and the seasonal variations in the stratosphere. Nevertheless, the information obtained from these observations is still limited; for example, only temperature data for 50°S–50°N/5–35 km and 50°S–50°N/20–120 km are obtained for GPS-RO and SABER, respectively.

[6] Another potentially useful data set for tidal studies is the global meteorological analysis (operational)/reanalysis data, which have been widely used for meteorological and climatological studies from the troposphere to the stratosphere over the last decade. The main advantage of these data sets is that various operational observations from the surface to the stratosphere (∼50 km) are assimilated into self-consistent first-principle models, leading to uniformly gridded and globally available data for several variables (e.g, temperature, wind, geopotential) up to the stratosphere–lower mesosphere (1–0.1 hPa in pressure; see Table 1 for details on each reanalysis). These data sets are 3-hourly or 6-hourly, so that they are suitable for tidal studies from a global perspective. In fact, several studies examined surface pressure tides, using (re)analyses [*van den Dool et al.*, 1997; *Dai and Wang*, 1999; *Ray*, 2001; *Ray and Ponte*, 2003; *Saha et al.*, 2010].

[7] Here it should be noted that (re)analysis data heavily depend on models (not on observations), particularly in the stratosphere and the mesosphere, where there are limited operational observations assimilated. Thus, validation is needed before using (re)analyses in this altitude region. However, very few validation studies, which are introduced in the following paragraph, have been conducted in this region. This is partly because there were only a few observational data sets that were independent of (re)analyses (i.e., not assimilated).

[8] From the troposphere to the lower stratosphere (below 22 km), *Sakazaki et al.* [2010] compared horizontal diurnal winds in six reanalyses with those observed with the middle atmosphere (MU) radar at (35°N, 136°E) for 23 years and showed that reanalyses reproduce diurnal winds reasonably well. *Pirscher et al.* [2010], using the National Centers for Environmental Prediction (NCEP) and the European Centre for Medium-range Weather Forecasts (ECMWF) forecast data (not (re)analysis data) for two years, also showed that they are in agreement with COSMIC data between 8 km and 35 km. On the other hand, *Swinbank et al.* [1999] compared the DW1 in GEOS-2 (an old version of GEOS-5) with that in MLS to show that the stratospheric amplitudes in GEOS-2 are smaller than those in MLS due to the assimilation of temperature data from TIROS Operational Vertical Sounder (TOVS).

[9] Since 2002, the SABER instrument on TIMED spacecraft has been observing temperatures from 20 km to 120 km.

**Table 2.** Assimilated Satellite Observation Data Related to the Stratospheric Temperature Profiles During 2002–2006 and Their Assimilation System

| Data Set | Assimilated Data | Assimilation System |
|---|---|---|
| MERRA | TOVS/ATOVS[a], EOS-Aqua[a] | 3D-Var |
| ERA-Interim | TOVS/ATOVS[a], EOS-Aqua[a], GPS-RO (CHAMP)[b] | 4D-Var |
| CFSR | TOVS/ATOVS[a], EOS-Aqua[a], GPS-RO (CHAMP)[b] | 3D-Var |
| JRA25 | TOVS/ATOVS[a] | 3D-Var |
| NCEP1 | TOVS/ATOVS[c] | 3D-Var |
| NCEP2 | TOVS/ATOVS[c] | 3D-Var |

[a]Radiance data are assimilated.
[b]Refractivity information are assimilated.
[c]Retrieved temperature data are assimilated.

Because the local time of the SABER measurements varies slowly from day to day, tidal variations can be deduced from these data sets [e.g., *Zhang et al.*, 2006]. Note that SABER data are not assimilated in reanalyses, making it possible to use SABER data to evaluate reanalysis data. The purposes of this study are, first to compare diurnal temperature tides in reanalyses with those in SABER for five years between 2002 and 2006 to assess whether reanalysis data can be used for tidal studies, and then to investigate the characteristics of the diurnal temperature tides from the troposphere to the lower mesosphere for the whole latitude range mainly using reanalyses. One of the concerns about the SABER data is the sampling issue related to the slow local time precession of the satellite [e.g., *Zhang et al.*, 2006; *Xu et al.*, 2007, 2009]. This issue will also be examined by using reanalyses. In addition, the results from the Global Scale Wave Model (GSWM), which are widely used in tidal studies, are assessed for the DW1 in the lower atmosphere.

[10] In this paper, we first compare the horizontal/vertical structures of diurnal tides including the DW1, determined from SABER and reanalysis data. At the same time, the sampling issues are examined by comparing diurnal tides from reanalysis data sampled following the SABER measurements with those from all available reanalysis data. Then, by using these data as well as GSWM09 results, the characteristics of diurnal tides (particularly the DW1) are examined in detail. We focus on the results from MERRA data, while the results from other reanalysis data are briefly described. The remainder of the manuscript is organized as follows. Sections 2 and 3 describe the data sets and analysis methods, respectively. Sections 4 shows the results of the diurnal component including the DW1 for SABER, reanalyses and GSWM, and discusses the sampling issues in SABER. Section 5 summarizes the main findings. In a companion paper, the underlying dynamics of DW1 for basic features, vertical structures from the tropical troposphere to the lower stratosphere, and seasonal variations from the tropical stratosphere to the lower mesosphere, will be investigated.

## 2. Data Sets

### 2.1. SABER

[11] The SABER instrument was launched onboard the TIMED satellite on December 7, 2001. It measures $CO_2$ infrared limb radiance from approximately 20 km to 120 km altitude and retrieves the kinematic temperature profiles. In this study, Version 1.07 temperature data on pressure levels [*Remsberg et al.*, 2008] from March 2002 through December 2006 for five years are analyzed. The latitude coverage on a given day extends from about 53° in one hemisphere to 83° in the other. About every 60 days, the satellite performs yaw maneuvers so that for the region polewards of 53°, data are obtained every 60 days. The local time of SABER measurements changes by about 12 min from day to day, so that the diurnal local-time variations can be examined by collecting data for 60 days (120 days) in the region of 53°S–53°N (poleward of 53°N and 53°S). In this study, the data at 50°S–50°N, where sampling is unaffected by the yaw maneuvers, are used for investigating diurnal tides. Before the further analysis as detailed in section 3, data have been averaged in bins of 5° in latitude and 2 km in log-pressure vertical coordinates ($z^*$) defined as $z^* = -H\log(p/p0)$, where $H = 7$ km is the approximate scale height, $p$ is pressure level and $p_0 = 1000$ hPa is the reference pressure. Hereafter, $z^*$ (km) is simply referred as "altitude".

### 2.2. Reanalysis Data

[12] We use six reanalysis data sets (see Table 1): (1) the Modern Era Retrospective analysis for Research and Applications (MERRA) [*Rienecker et al.*, 2011], (2) the ECMWF reanalysis (ERA-Interim) [*Dee et al.*, 2011], (3) the NCEP Climate Forecast System Reanalysis (CFSR) [*Saha et al.*, 2010], (4) the Japanese 25-year reanalysis by Japanese Meteorological Agency (JMA) and the Central Research Institute of Electric Power Industry (CRIEPI) (JRA25) [*Onogi et al.*, 2007], (5) the NCEP/National Center for Atmospheric Research (NCAR) reanalysis (NCEP1) [*Kalnay et al.*, 1996], and (6) the NCEP and Department of Energy (DOE) Atmospheric Model Intercomparison Project (AMIP-II) reanalysis data (NCEP2) [*Kanamitsu et al.*, 2002].

[13] The temporal resolution of the MERRA data set is eight-times daily at 0000, 0300, 0600, 0900, 1200, 1500, 1800, 2100 UTC, while the other five reanalyses resolutions are four-times daily at 0000, 0600, 1200, and 1800 UTC. The horizontal spacing for each data set is the following: 0.5° × 0.5° for CFSR, 1.25° × 1.25° for MERRA and JRA25, 1.5° × 1.5° for ERA-Interim, and 2.5° × 2.5° for NCEP1 and NCEP2. The number of pressure levels for each data set is the following: 42 for MERRA, 37 for ERA-Interim and CFSR, 23 for JRA25, and 17 for NCEP1 and NCEP2, with top levels at 0.1 hPa for MERRA, 1 hPa for ERA-Interim and CFSR, 0.4 hPa for JRA25, and 10 hPa for NCEP1 and NCEP2. The details about the model used in each reanalysis are also shown in Table 1.

[14] Reanalyses assimilate 6-hourly observations, so that the signals of observed diurnal variations are included. In the stratosphere during 2002–2006, radiances (MERRA, ERA-Interim, CFSR and JRA25) or retrieved temperatures (NCEP1 and NCEP2) from TOVS and Advanced TOVS (ATOVS), radiances from EOS-Aqua (MERRA, ERA-Interim and CFSR), and GPS-RO (ERA-Interim and CFSR) are assimilated (see Table 2). These observations provide data only up to ∼50 km; but they greatly influence further upper regions through model calculations (J. Bacmeister, personal communication, 2010). For data assimilation, JRA25, NCEP1 and NCEP2 use 3D-Variational technique (3D-Var) [e.g., *Japan Meteorological Agency*, 2002; *Parrish and*

*Derber*, 1992], while ERA-Interim uses 4D-Var [e.g., *Courtier et al.*, 1994]. MERRA and CFSR uses 3D-Var based on the Grid-point Statistical Interpolation scheme (GSI) [e.g., *Wu et al.*, 2002]. Furthermore, MERRA uses the incremental analysis update (IAU) approach [*Bloom et al.*, 1996] to avoid shocking the model calculations at 6-hourly assimilation.

[15] We analyze the reanalyses data for the five-year period from 2002 to 2006, the same period that characterizes the SABER data. It should be again noted that SABER data are independent of these reanalyses; that is, they are not assimilated in these reanalyses.

### 2.3. GSWM09 Data

[16] In addition to these observational data, DW1 temperature tides from the GSWM are presented in section 4.2. The GSWM is a 2-D (latitude and altitude) linear numerical tidal model [*Hagan et al.*, 1995, 1999]. We use results from the latest version (GSWM09) reported by *Zhang et al.* [2010a, 2010b], who ran the GSWM with the tropospheric heating derived from International Satellite Cloud Climatology Project (ISCCP) radiative heat fluxes and Tropical Rainfall Measuring Mission (TRMM) latent heating profiles from 2002–2006, and with the stratospheric heating estimated from Halogen Occultation Experiment (HALOE) measurements made during 1992–1997 (below 50 km) and Microwave Limb Sounder (MLS) measurements made during 1991–1993 (above 50 km) [see *Hagan et al.*, 1999]. Note that the period used to calculate tropospheric heating (2002–2006), which is most important for DW1, is the same as the analysis period for the observation data (reanalysis/SABER), so that we can directly compare the results between observations and GSWM09. The validation of GSWM data in the lower atmosphere is important because GSWM data have often been used as a reference of realistic tides (e.g., as the lower boundary tidal condition (at 30 km) for the TIME/GCM [*Liu et al.*, 2007]) without detailed assessments in the lower atmosphere. Unlike SABER and reanalyses, GSWM09 data are provided in geometric altitude.

## 3. Methods

[17] For temporally continuous data such as atmospheric radar data [e.g., *Sakazaki et al.*, 2010], diurnal variations are obtained simply by producing the local-time composite using all data in the period concerned. In contrast, for SABER data, due to the slow local time precession of the satellite, tidal components derived from the "simple local-time composite" could suffer from sampling issues due to changes in the background (longer than a day) temperature with time [*Forbes et al.*, 1997]. To avoid this problem, we extract diurnal variations following the method proposed by *Forbes et al.* [2008], which is described below.

[18] First, we prepare daily data averaged in bins of 24° in longitude, 5° in latitude, and 2 km in log-pressure altitude, for each ascending and descending node. In this case, each bin stores at least one data point every day (this is because the number of orbit is 15 per day and thus the measurement is made every 24° (i.e., 360°/15 = 24°) in longitude for a given day). Next, a time series of 60-day running mean temperatures is calculated for each bin (both ascending and descending data are used for calculation). The 60-day data cover 24 LT so that the 60-day running mean is regarded as the daily mean component with no tidal information. Note that as for SABER, the 60-day window is the minimum amount of time needed for calculating the daily mean. Then, the 60-day running means are subtracted from the original temperatures at each day to obtain a 5-year time series of residual temperatures, for each bin and for each ascending and descending node. At this stage, it is expected that the effects of changes in background temperature have been reduced. Finally, for each month at each longitude-latitude-altitude bin, the residuals (i.e., 60-day data centered on 15th of the month from the five years) are binned and averaged within 1-hr local time bins, and the diurnal harmonic component (i.e., amplitude and phase) is extracted using the least square fitting technique. The actual fitting accounts for the diurnal and semidiurnal harmonic components. Here, the phase is the local time when the component maximizes.

[19] For the reanalysis data sets, we determine the diurnal component in two different ways. One is obtained from the SABER perspective. That is, we prepare a subset of the reanalysis data that correspond to the times and locations when and where the SABER measurements are made. We extract the data at the closest grid point to the SABER measurements, while these data are interpolated onto the SABER measurement altitude levels and times, respectively using a cubic spline method. Then, the reanalysis diurnal component is determined using exactly the same method described above for SABER. This diurnal component is denoted as S-; e.g., S-reanalysis or S-MERRA.

[20] The second diurnal component is obtained using all of the reanalysis data. That is, we develop local-time composites using 60-day 3(6)-hourly five-year averages for each month and extract the diurnal component, which we denote as A-; e.g., A-reanalysis or A-MERRA.

[21] To summarize, we prepared three sets of diurnal temperature for each month: (1) SABER, (2) S-reanalysis and (3) A-reanalysis. Comparisons between SABER and S-reanalysis allow us to validate the diurnal component in the reanalysis data. Comparisons between S-reanalysis and A-reanalysis quantify the sampling issues associated with the SABER measurements. Thereafter, the migrating component (i.e., the DW1) is extracted from the diurnal component of SABER, S-reanalysis and A-reanalysis, using the method proposed by *Haurwitz and Cowley* [1973]. The results are discussed in section 4.2. For the detailed examination of DW1 characteristics in section 4.2, we use A-reanalysis data from 30-day (not 60-day) data for each month.

[22] The comparisons in daily mean and standard deviation which is composed of all waves including tides are additionally made using SABER and S-reanalysis in Appendix A. This information aids the interpretation of our tidal intercomparisons.

## 4. Results

[23] In this section, we inter-compare and examine the diurnal temperatures from SABER, S-reanalyses and A-reanalyses. Also, we point out that there still remain sampling issues inherent in SABER measurements, even after removing the 60-day running mean. We focus on the reanalysis results from MERRA data due to its comparatively higher altitude extent and temporal resolution. In section 4.1,

diurnal component with all zonal wave numbers is examined, while in section 4.2 the DW1 is the focus with the results of GSWM09 being shown as well.

### 4.1. Diurnal Component With All Zonal Wave Numbers

[24] Figures 1 and 2 show longitude–latitude distributions of diurnal amplitude and phase, respectively, at 20, 30, 40, 50, and 60 km in January as derived from SABER data (left panels), S-MERRA data (middle panels) and A-MERRA data (right panels). In Figures 1a and 1b, considerably large amplitudes are detected poleward of ~40°N between 20 and 50 km. The largest values of 5–8 K appear at 40–50 km. However, these signals are not observed in Figure 1c. The phase difference is also large between S-MERRA and A-MERRA data for this region (Figures 2b and 2c). These findings suggest that the SABER diurnal component in this latitude–altitude region suffers from sampling issues, even though 60-day running mean has been removed in advance. By analyzing the results in other months, it is found that the difference between SABER/S-MERRA and A-MERRA is large at middle latitudes in the winter hemisphere (not shown). Other reanalyses show similar results for the difference between S- and A-reanalyses.

[25] In contrast, the region of 50°S–30°N is considered to be free from the sampling issues in January, because the difference between S-MERRA and A-MERRA is negligible (Figures 1 and 2). However, the amplitude of these "true" diurnal tides shows a quantitative difference between SABER and S-MERRA. Figure 3 shows vertical profiles of differences in diurnal amplitudes (Figures 3a–3c) and phases (Figures 3d–3f) between SABER and S-reanalysis, for three different latitude regions. In order to remove the effects of sampling issues in the winter hemisphere, the values at 50°S–20°S (20°N–50°N) are calculated only using summer data from October–March (April–September), while the values at 20°S–20°N are calculated using data from all months. The amplitude differences are <0.5 K below 40 km but increase with altitude to 1–2 K at 50–60 km. The relative ratio of difference is <20% below 40 km while it reaches 30–50% at 50–60 km. In contrast, the difference in phase is <2 hr for the whole altitude region. The large amplitude differences at 50–60 km are also confirmed in Figure 1. Note that the quantitative difference in amplitudes shown in Figure 3 does not depend on longitude. Here it is interesting that the standard deviation composed of all waves including tides does not change between SABER and reanalyses (Figure A2 in Appendix A), compared to that of diurnal tides. When comparing the results of tides among the reanalyses (Figure 3), the stratospheric amplitudes in CFSR at middle latitudes are ~0.5 K smaller than the others. However, the difference among the reanalyses in the stratospheric diurnal tide is relatively small, compared to the large variability among the reanalyses in the daily mean (Figure A1 in Appendix A).

[26] Note that MERRA results have been obtained with 3-hourly data. It is confirmed that the results do not change even if 6-hourly sampled MERRA data are used (not shown). The difference in amplitude (phase) between the 3-hourly and 6-hourly results is <10% (<1 hr) both for S-MERRA and A-MERRA. Thus, it is suggested that the difference between SABER and reanalysis does not depend on the time resolution of the reanalyses. We also examined SABER and S-reanalysis obtained from data at reanalysis measurement time (i.e., data are picked up 3-hourly in UT for MERRA) but the results did not change (not shown).

[27] Apart from the quantitative differences, the qualitative features of the SABER and MERRA diurnal tides are similar. As seen in Figures 1 and 2, at 50°S–30°N, the amplitudes and phases are roughly zonally uniform at all altitudes, indicating the dominance of migrating component (i.e., DW1) in both data sets. Detailed features of DW1 are described below in section 4.2. Superposed on these zonally uniform features, the amplitudes at 20–40 km have three or four peaks over the tropics (e.g., at 30 km, the maximum over the tropics appear at 330°E–30°E, 120°E and 240–270°E). At 50 km, we observe another clear wave-4 pattern in the amplitudes at midlatitudes in the Southern Hemisphere (SH). This pattern is also discernable at 40 km and 60 km, although the amplitudes are smaller than at 50 km. The phase also shows a corresponding wave-4 structure in the SH at 40–50 km. This wave-4 pattern is attributed to the DW1 and the propagating zonal wave number 3 component (DE3). That is, the amplitude ($A$) of superposition of two components: DW1 ($C\exp(i(\omega t+\lambda-\phi_C))$) and DE3 ($D\exp(i(\omega t-3\lambda-\phi_D))$), is represented as,

$$A = |C\exp(i(\omega t+\lambda-\phi_C)) + (D\exp(i(\omega t-3\lambda-\phi_D))| = C\sqrt{1+\left(\frac{D}{C}\right)^2+2\frac{D}{C}\cos(4\lambda-(\phi_C-\phi_D))}, \quad (1)$$

resulting in four amplitude peaks in longitudes unless D/C is negligibly small. Here, $C$ and $D$ are amplitudes of DW1 and DE3, respectively; $\omega = 2\pi/24$ (hour$^{-1}$); $t$ is universal time (UT) in hours; $\lambda$ is longitude in radian; $\phi_C$ and $\phi_D$ are phases of DW1 and DE3 respectively. In the present case, $C \sim 2$ K (Figure 5c) and $D \sim 1$ K (see Figure 4), resulting in the wave-4 pattern of $A$ which takes a value of 1–3 K from equation (1), as observed in Figure 1c. The existence of DE3 is demonstrated in Figure 4 which shows the time series in UT for diurnal non-migrating temperature tides at 50 km in January as derived from A-MERRA data. We see that a clear zonal wave number 3 pattern is traveling eastward with time in the SH (20°S–50°S). This DE3 and the DW1 interfere each other, mainly producing amplitude maxima/minima distributions in the SH in Figure 1. These wave-4 patterns in the amplitudes in the SH are most clear in this season. In July, a wave-3 pattern in the amplitudes is discernable in the Northern Hemisphere (NH) although it is less organized (not shown).

### 4.2. Diurnal Migrating Component (DW1)

[28] In this subsection, the DW1 is examined. Figure 5 shows the latitude-altitude DW1 temperature amplitudes and phases, respectively, for SABER, S-MERRA and A-MERRA during January. We see that the considerably large amplitudes observed at 30–50°N, 35–55 km in SABER and S-MERRA are not observed in A-MERRA. This is due to the SABER sampling issues as discussed in the preceding section. Therefore, the DW1 deduced from SABER also has non-negligible aliasing effects particularly in the winter stratosphere. For other regions, as shown in section 4.1, the difference between S-MERRA and A-MERRA is small, indicating negligible sampling issues. For these "true" DW1,

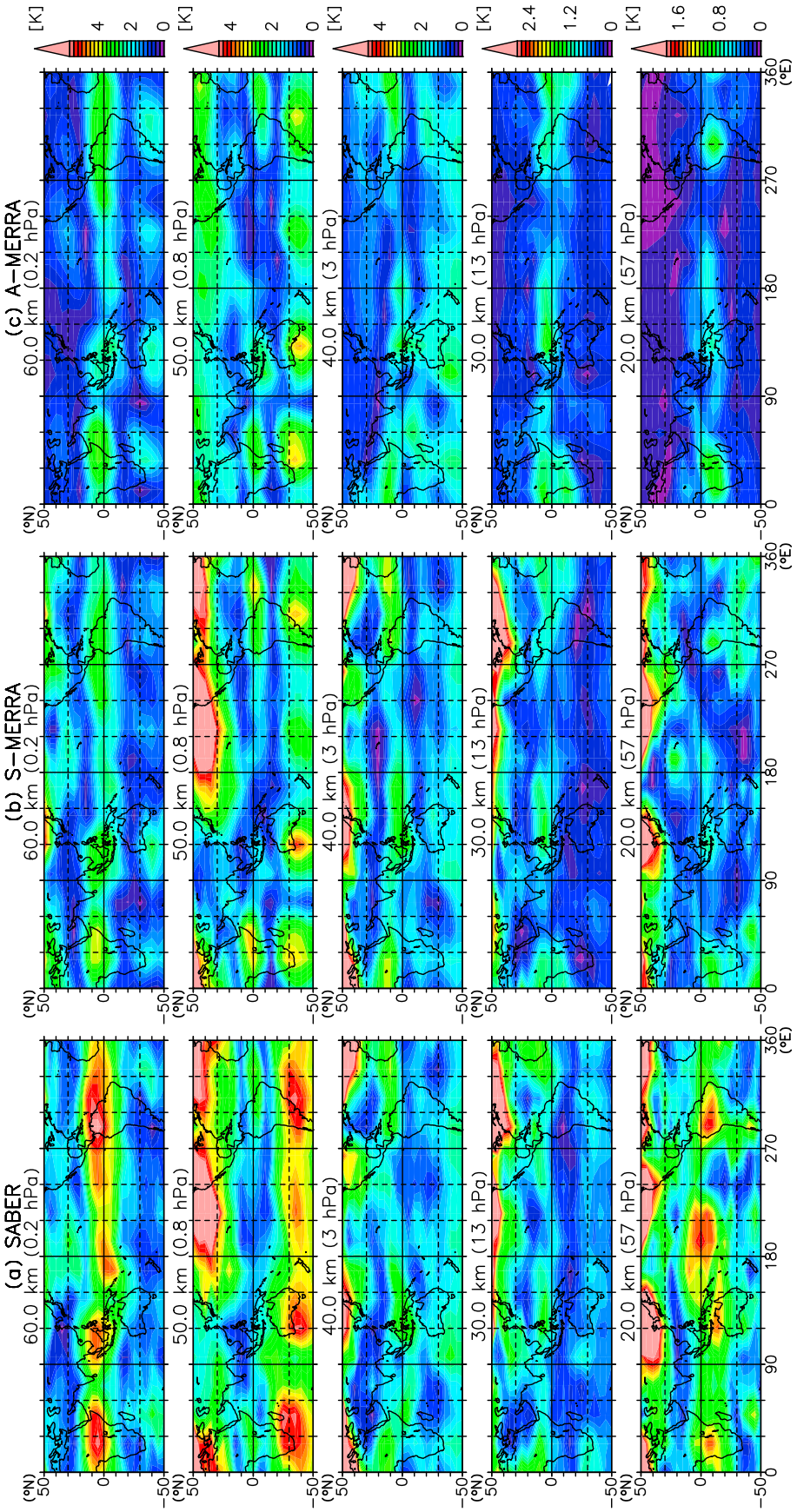


**Figure 1.** Longitude–latitude distributions of diurnal tidal amplitude of temperature in January at 20, 30, 40, 50 and 60 km as derived from (a) SABER data, (b) S-MERRA data, and (c) A-MERRA data. Color bars are shown at the right of each altitude panel. Color allocation is different with different altitude levels.

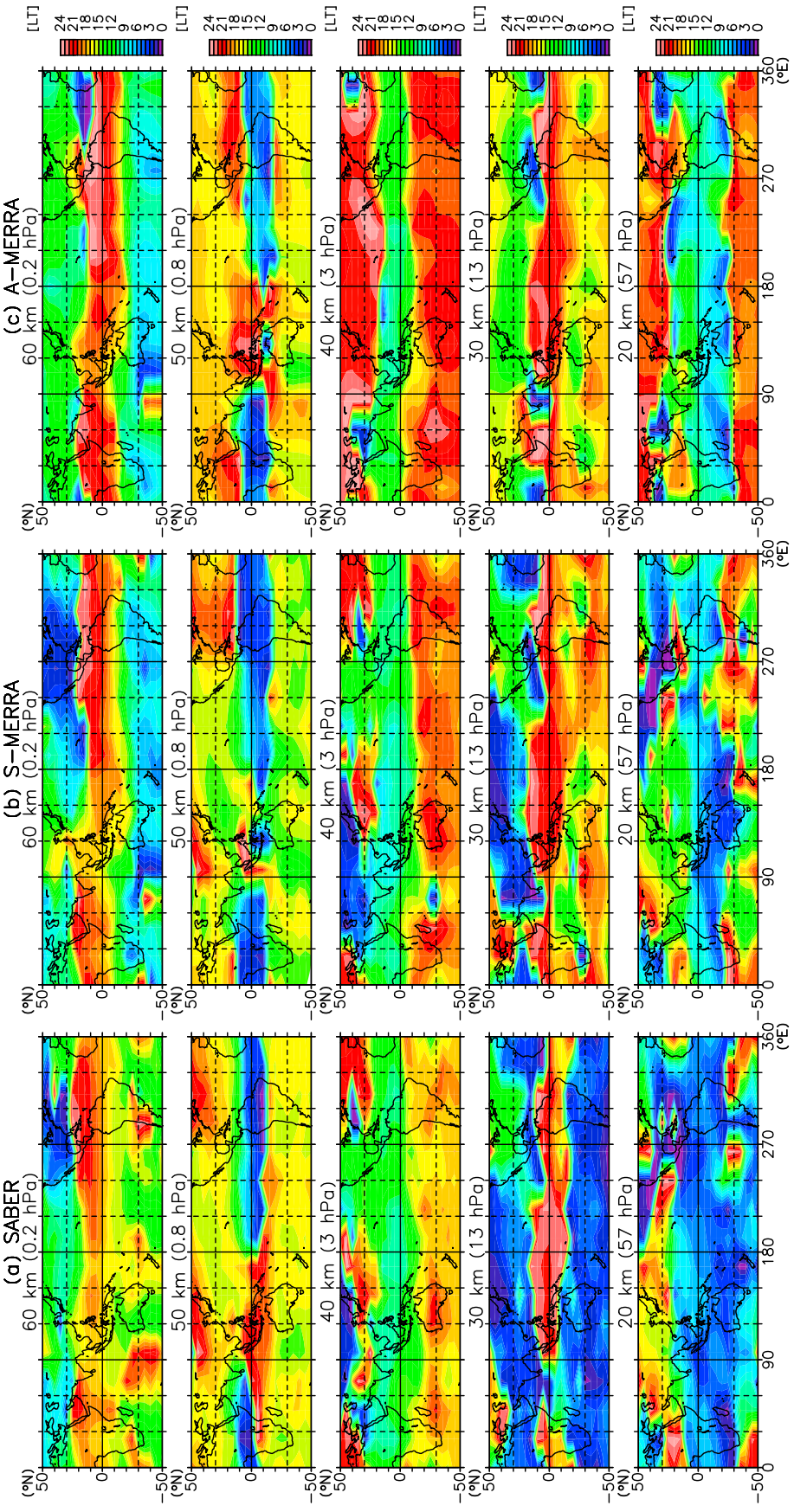


**Figure 2.** Same as Figure 1 but for phase.

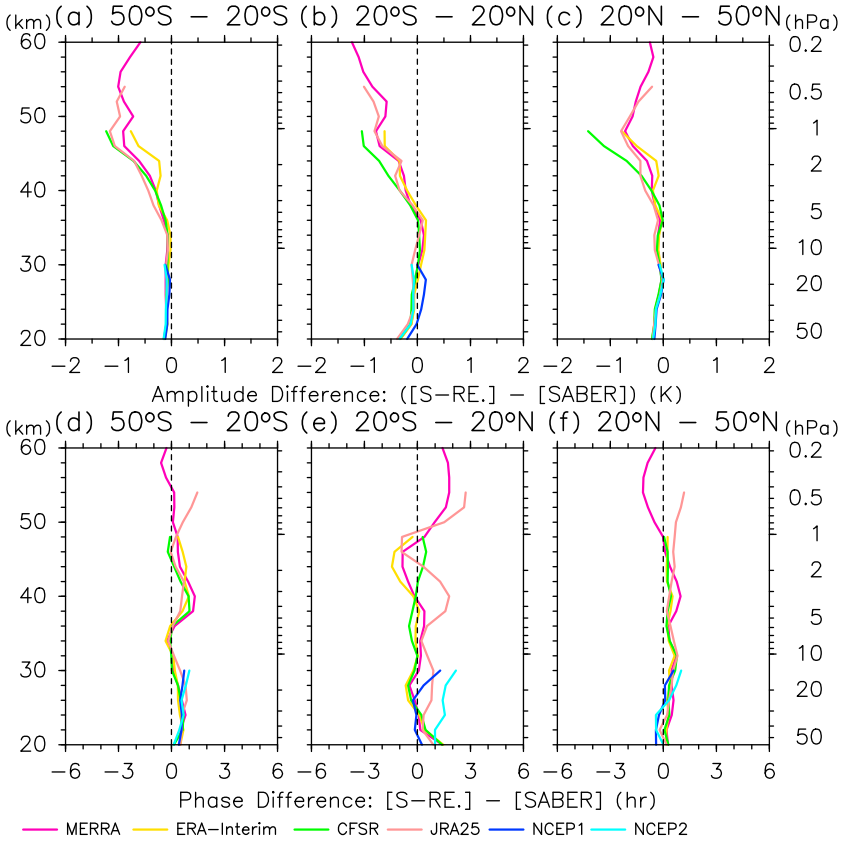


**Figure 3.** Vertical profiles of difference in (a–c) amplitude and (d–f) phase for diurnal tidal temperature, between SABER and S-reanalysis (S-reanalysis minus SABER), which is averaged for 2002–2006. Figures 3a and 3d are for 50°S–20°S, Figures 3b and 3e are for 20°S–20°N, and Figures 3c and 3f are for 20°N–50°N. Note that in order to remove the effects of sampling issues in the winter hemisphere, the values at 50°S–20°S (20°N–50°N) are calculated using summer data from October–March (April–September), while the values at 20°S–20°N are calculated using data from all months (see text for details). Purple curves are for MERRA, yellow curves are for ERA-Interim, green curves are for CFSR, light red curves are for JRA25, blue curves are for NCEP1, and light blue curves are for NCEP2.

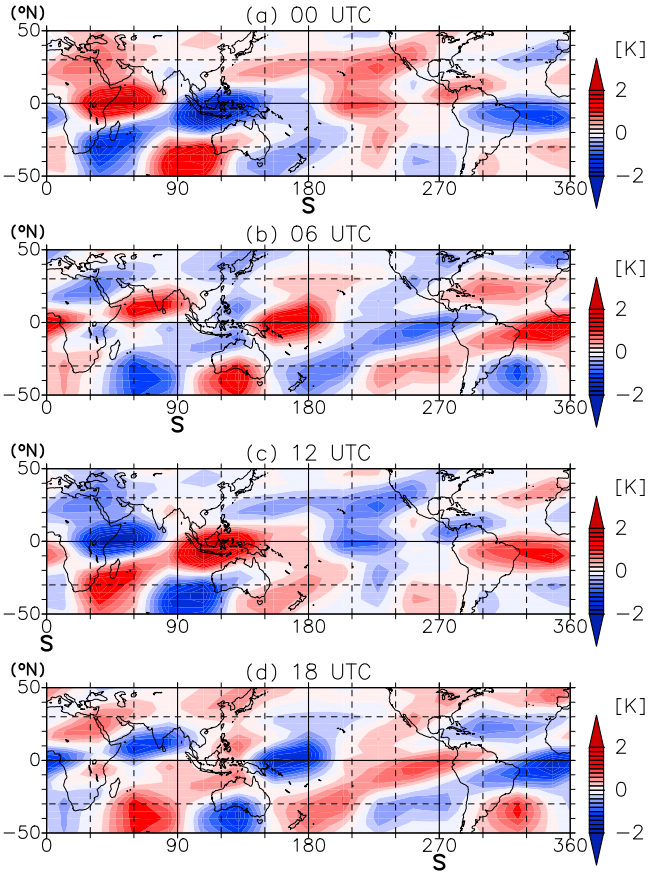


**Figure 4.** Time series of longitude–latitude distributions of diurnal non-migrating temperature tides at 50 km in January, as derived from A-MERRA data: (a) 00 UTC, (b) 06 UTC, (c) 12 UTC and (d) 18 UTC. "S" at the bottom of each panel shows the Sun motion. Color bar is shown on the right.

we see that the distributions of amplitude maxima/minima and those of phase in SABER are reproduced by MERRA quite well, although the stratospheric amplitudes are 30–50% smaller in S-MERRA than in SABER.

[29] Bearing in mind the SABER's sampling issues and the quantitative difference between SABER and A-MERRA, the latitudinal–vertical structures and their seasonal variations of DW1 are examined in detail for the whole latitude–altitude range in the lower atmosphere. Figures 6 and 7 show latitude–altitude distributions of amplitude and phase, respectively, of DW1 temperature in January, April, July and October, as derived from SABER, A-MERRA and GSWM09. As noted in section 3, hereafter A-reanalysis data is derived from 30-day data for each month. For SABER, data in January (July) are shown only for 50°S–30°N (30°S–50°N), where sampling issues are negligible. Again, the amplitude/phase distributions in SABER are basically reproduced by MERRA throughout the year. On the basis of this finding, we can examine the DW1 for the whole lower atmosphere using MERRA. MERRA results show that the characteristics are distinctly different between the tropics (30°S–30°N) and latitudes poleward of 30°. The amplitudes basically maximize in the tropics, where they increase with altitude, reaching 3–4 K in the lower mesosphere. A local minimum is seen at ∼50 km. In this latitude region, the phase shows a downward progression above the tropopause. The distributions of amplitudes/phases are nearly symmetric about the equator in April and October, while they exhibit anti-symmetric structure particularly in January and July. In January, for example, the amplitude in the tropics is larger in the SH at 20–30 km, in the NH at 30–40 km, in the SH at 40–50 km, and in the NH at 50–60 km. At midlatitudes, in contrast, double maxima of 2–3 K are seen in the upper stratosphere (40–50° at ∼50 km). The maximum in the summer hemisphere is larger than that in the winter hemisphere (see the panels for January and July). The phase in this region is almost constant with altitude at ∼18 LT throughout the year.

[30] The results of GSWM09 are compared with those from SABER/MERRA. The basic features found in SABER and MERRA are reproduced by GSWM09 reasonably well. However, we observe in GSWM09 that the tropical anti-symmetric structure in January and June is too weak and that the amplitude maximum in midlatitude upper stratosphere is 50–60% (30–50%) smaller than that in the SABER (MERRA). Also, the latitude extent where a vertical phase propagation occurs from the tropical stratosphere to the lower mesosphere is much broader in the GSWM09 (70°S–70°N) than in the SABER and MERRA (50°S–50°N). The possible reasons for these discrepancies will be discussed in our companion paper.

[31] We also show the DW1 results from different reanalyses. Figures 8 and 9 show latitude–altitude distributions of amplitude and phase, respectively, of DW1 temperature in January from ERA-Interim, CFSR, JRA25, NCEP1 and NCEP2 for A-reanalysis data. The basic structures in the stratosphere are similar among reanalyses (including MERRA shown in Figures 6b and 7b) both for amplitude and phase, although the amplitude at ∼30 km is smaller in the NCEP1 and in the NCEP2 than in the other reanalyses and the amplitude maxima in midlatitude stratosphere are relatively smaller in CFSR and JRA25 (also see Figure 3). Other months show similar results for the above findings (not shown).

[32] Next, the vertical structure from the tropical troposphere to the lower stratosphere is examined. Figure 10 shows vertical profiles of amplitude and phase of DW1 temperature at the equator (0°N) in January for the different data sets. Although the SABER data coverage is limited for this altitude region, most reanalysis data sets (MERRA, ERA-Interim and CFSR) show that the amplitude is almost constant at ∼0.3 K up to ∼15 km, and shows a local maximum at ∼20 km. Above 25 km, the amplitude shows an exponential growth. The phase is almost constant at ∼18 LT up to ∼15 km, and shows a downward progression above ∼15 km with a vertical wavelength of ∼25 km, indicating an upward propagating tide. These features are observed basically throughout the year (not shown). These observed features are quantitatively consistent with the observed finding from GPS-RO data [*Zeng et al.*, 2008] and are reproduced by GSWM09 reasonably well (dashed curves in Figure 10). It is noted that the amplitude structures of JRA25, NCEP1 and NCEP2 are different from those of the other data sets above 15 km.

[33] Finally, the seasonal variations of DW1 are examined. We found two distinct signatures of seasonal variation in the stratosphere as seen in Figure 6. First, the amplitudes in the

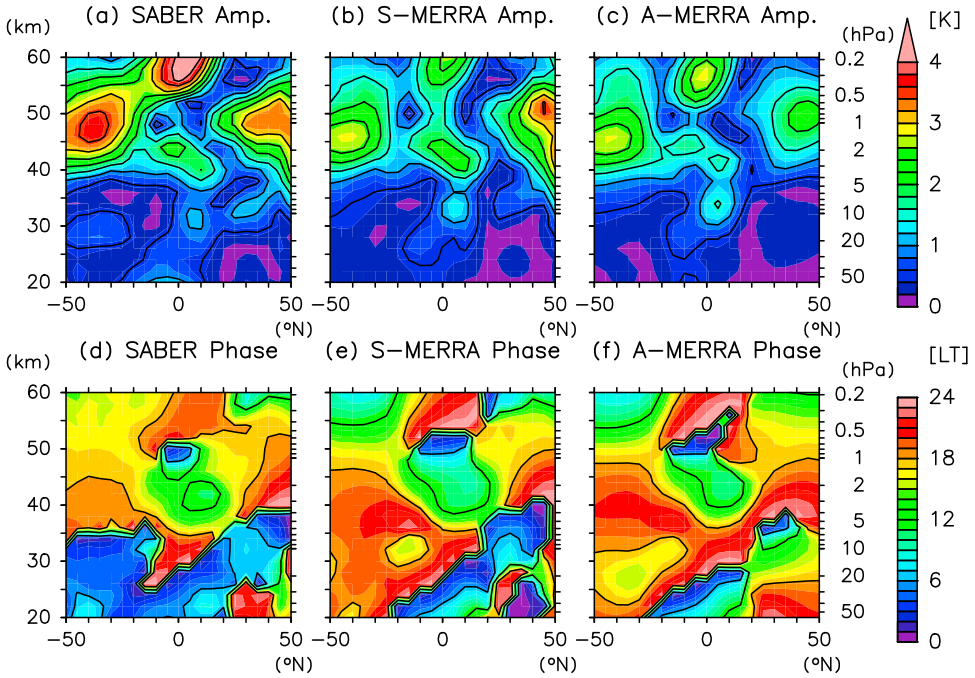


**Figure 5.** Latitude–altitude distributions of diurnal migrating (a–c) amplitude and (d–f) phase in January. Figures 5a and 5d are from SABER data, Figures 5b and 5e are from S-MERRA data, and Figures 5c and 5f are from A-MERRA data. Contour interval is 0.5 K for Figures 5a–5c and 6 hr for Figures 5d–5f. Color bars are shown on the right.

midlatitude upper stratosphere are larger in the summer hemisphere than in the winter hemisphere. Second, the DW1 amplitudes at 50–60 km are largest in the tropics in January. The latter feature is further discussed in the following. Figure 11 shows tropical latitude versus month distributions of DW1 temperature amplitudes at different altitudes for 30°S–30°N, as derived from SABER, MERRA and GSWM09. SABER and MERRA basically show similar features in the stratosphere. Above 20 km, the amplitude maximizes twice in January–February and in July–August–September. These maxima are largely anti-symmetric with respect to the equator; that is, the maxima occur at 5–10°N/S. The characteristic seasonal variations are consistent with previous studies (above ∼30 km) with the MLS [*Wu et al.*, 1998], GPS-RO [*Zeng et al.*, 2008; *Xie et al.*, 2010] and SABER [*Mukhtarov et al.*, 2009; *Huang et al.*, 2010]. It is also found from MERRA data (at ∼10 km) that the above seasonal variations are not observed in the troposphere, where the amplitude basically maximizes in the summer hemisphere. GSWM09 show similar results to SABER and MERRA; however, as noted in Figures 6 and 7, the tropical anti-symmetric behavior during solstice is considerably smaller in the stratosphere. The ERA-Interim and CFSR reanalyses results show similar seasonal variations to MERRA; JRA25 shows qualitatively similar results, although the amplitudes are reduced at some altitudes. In contrast, the seasonal variations in NCEP1 and NCEP2 are totally different at ∼30 km, which is at the top of their altitude range (not shown).

## 5. Discussion and Concluding Remarks

[34] We analyzed diurnal tides in temperature using 2002–2006 data from SABER and six reanalysis data sets. We examined sampling issues through comparisons between S-MERRA and A-MERRA data, and found that the diurnal component in the winter stratosphere extracted from SABER data suffers from sampling issues, even though the 60-day running mean was removed in advance. We further investigate the causes of these sampling issues below. Figure 12 shows the time series of temperature at two grid points (35°N, 216°E) and (35°S, 216°E), both at 50 km in January, 2003. The former location suffers from sampling issues, while the latter is free from the problem as previously indicated in the discussion of Figure 1. A diurnal component of order ∼5 K amplitude is dominant at both locations (Figure 12). Superposed on the diurnal component, the background temperature in the NH shows a strong variability with a timescale less than ∼60 day. This is caused by strong Rossby-wave activity in the winter Hemisphere. The variability of this timescale is not captured by the 60-day running mean (thick solid line) and thus spuriously contaminated into the observed diurnal component. In contrast, there is little variability in the background temperature for the SH during this period, enabling the satellite to detect the diurnal component without sampling issues. The strong (weak) variability due to Rossby waves at the winter (summer) hemisphere midlatitudes is observed almost every year during 2002–2006 (not shown). It is suggested that tides extracted from satellite observations should be viewed with caution, when there is strong subseasonal variability of the atmosphere. Further experiments for a simple case show that during a particular month, the background temperature variability with the period of 30–60 days, which are strong in winter hemisphere stratosphere, seems most related to the sampling issues (see Appendix B for details). As discussed in Appendix B, the variations with a period of 10 days, which

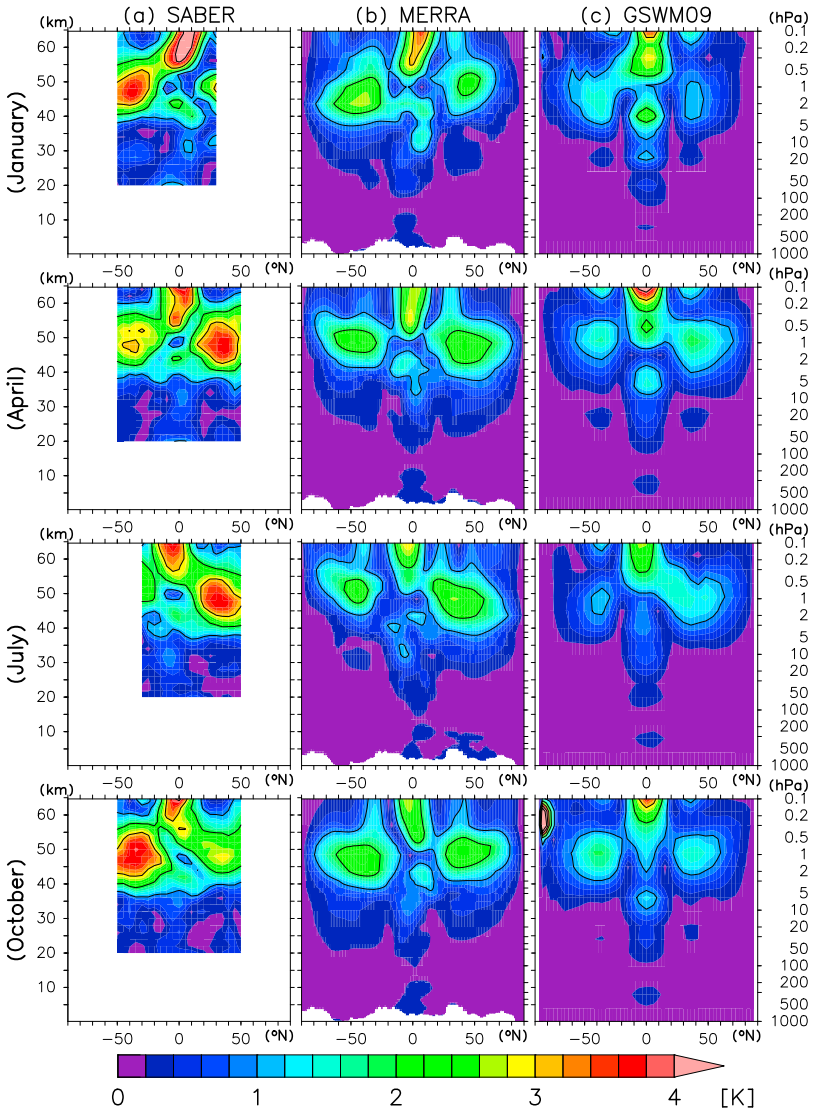


**Figure 6.** Latitude–altitude distributions of the amplitude for DW1 temperature as derived from (a) MERRA data, (b) SABER data, and (c) GSWM09 data. From top to bottom, panels are for January, April, July, and October. For Figure 6a, data in January (July) are shown only for 50°S–30°N (30°S–50°N), where sampling issues are negligible. See text for details. Color bar is shown at the bottom. Contour interval is 1 K.

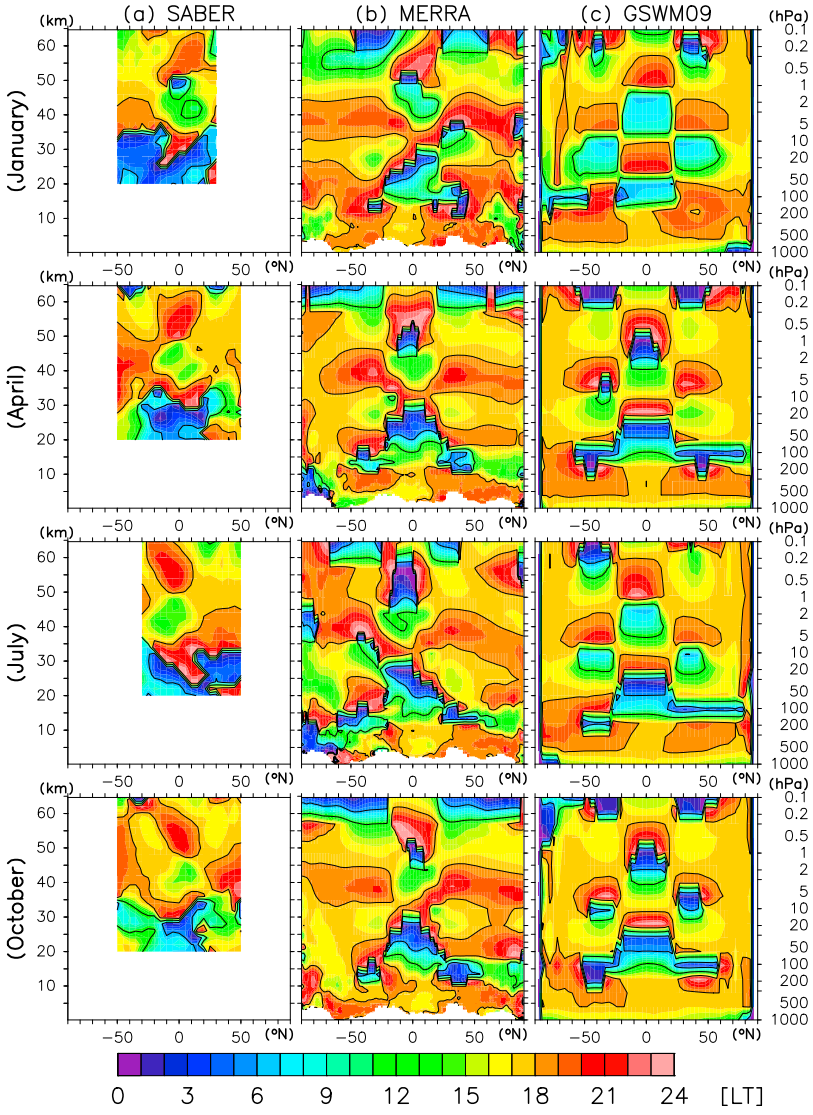


**Figure 7.** Same as Figure 6 but for phase. Contour interval is 6 hr.

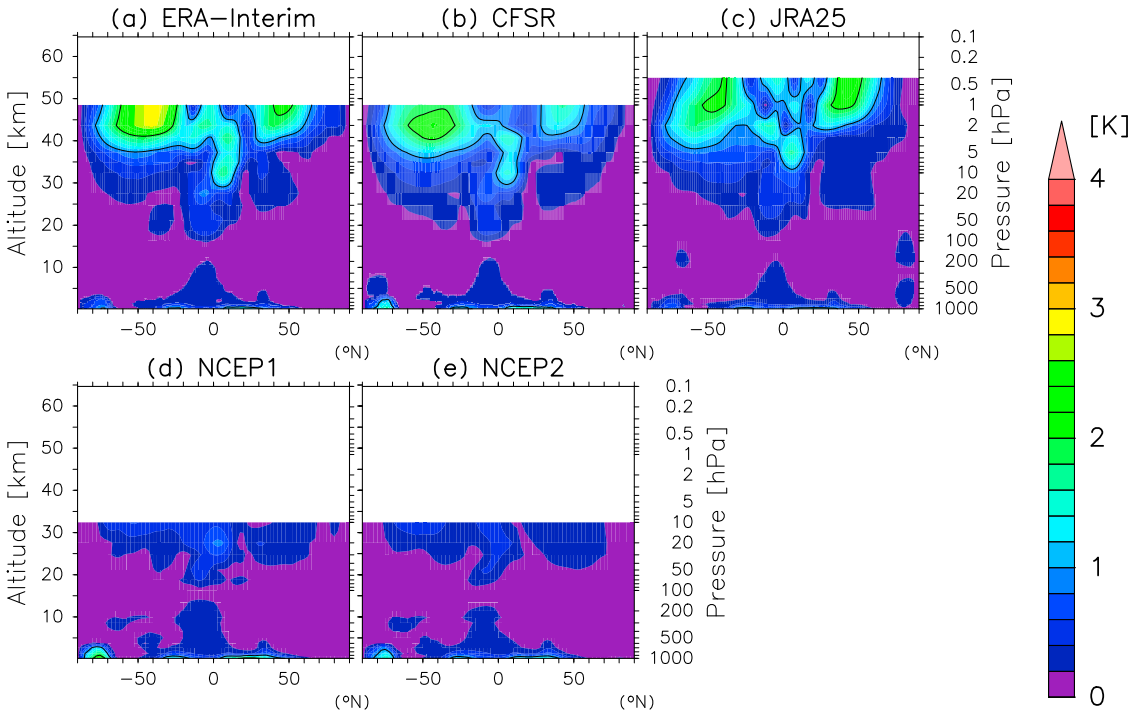


**Figure 8.** Same as Figure 6 but for the amplitude for DW1 temperature in January as derived from the A-reanalysis data: (a) ERA Interim, (b) CFSR, (c) JRA25, (d) NCEP1 and (e) NCEP2. Contour interval is 1 K. Color bar is shown on the right.

appear to be most dominant in Figure 12, are not substantially aliased into the diurnal component.

[35] The lower and middle atmosphere outside of the winter hemisphere stratosphere is largely free from sampling issues. With the comparison between SABER and S-reanalysis data, it is shown that the reanalyses capture the diurnal tidal features (i.e., horizontal/vertical distributions of amplitude and phase and their seasonal variations) observed by SABER

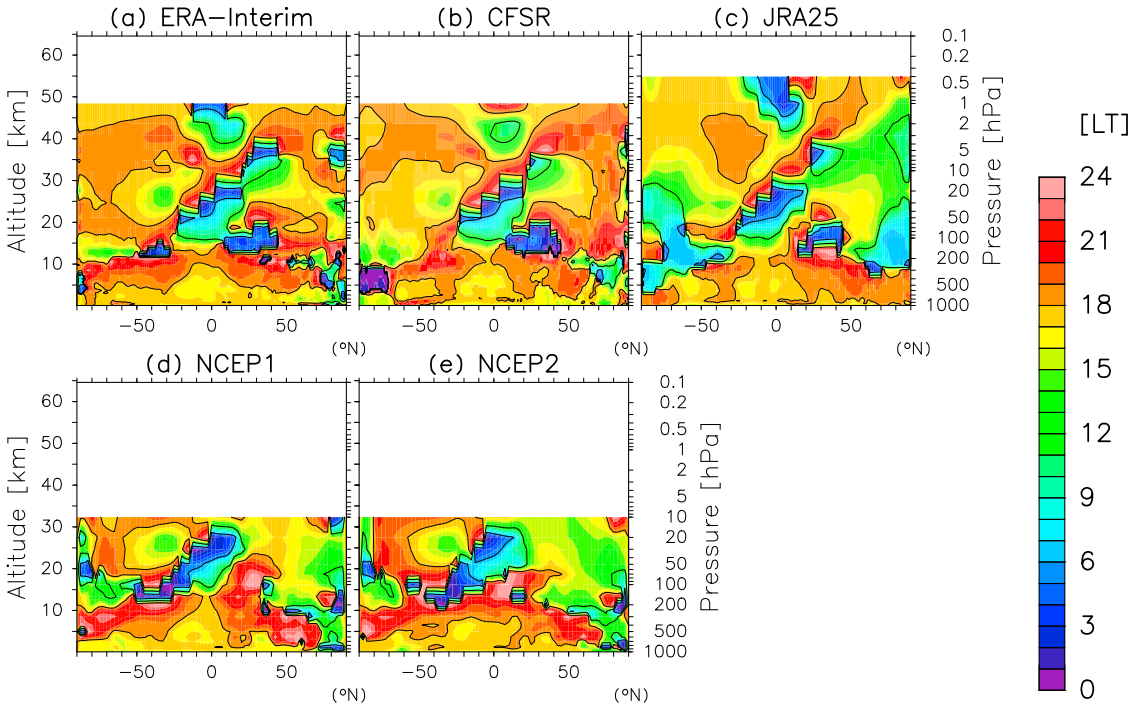


**Figure 9.** Same as Figure 8 but for phase. Contour interval is 6 hr.

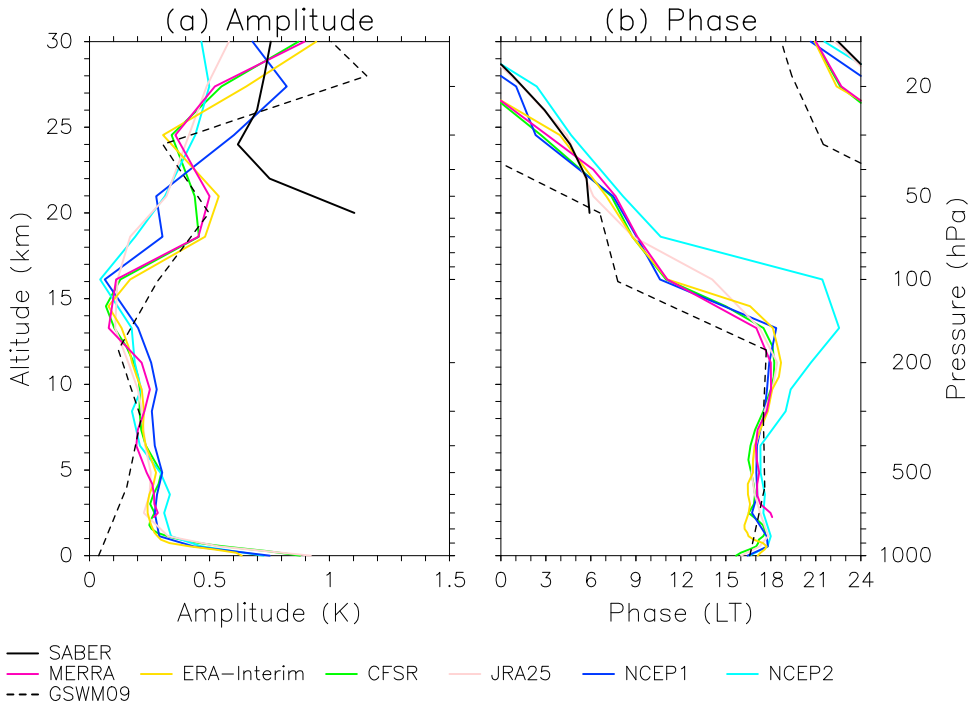


**Figure 10.** Vertical profiles of (a) amplitude and (b) phase of DW1 temperature at the equator from SABER, A-reanalyses and GSWM09. Solid black curves are for SABER and solid dotted curves are for GSWM09. The color allocation for reanalyses is the same as Figure 3.

reasonably well, except that amplitudes of reanalyses from the upper stratosphere to the lower mesosphere are 30–50% smaller than those of SABER. Thus, it is suggested that reanalyses can be used for tidal studies at least from a qualitative perspective. The reanalysis data sets could be used as lower boundary conditions to account for tides in upper atmosphere models (e.g., TIME-GCM), or for revealing the subseasonal tidal variability that cannot be captured by satellite observations such as the SABER.

[36] The plausible causes of diurnal amplitude difference between SABER and reanalyses from the upper stratosphere to the lower mesosphere are complex. They could be damping effects (i.e., "sponge layer") in the upper part of the forecast model used for the reanalyses or compatible biases of assimilated radiances from different satellite instruments (S. Pawson, personal communication, 2011). TOVS data assimilation might be also a possible candidate, as suggested by *Swinbank et al.* [1999]. It is worth noting that the standard deviation which is composed of all waves including tides does not change between SABER and reanalyses, compared to that for diurnal tides. Experiments with and without data assimilation using a model whose upper boundary is sufficiently high might provide additional clues.

[37] A clear wave-4 structure in the diurnal amplitudes was discovered in the SH midlatitude region at 40–60 km. This may be explained by the superposition of DW1 and DE3 components. The DE3 was reported in the tropics in previous studies, and was attributed to wave-4 tropospheric diabatic heating in the tropics that is influenced by land-sea distributions [e.g., *Tokioka and Yagai*, 1987; *Williams and Avery*, 1996a]. The DE3 in the SH upper stratosphere, however, is a new observational finding as far as the authors know. The midlatitude maximum may be partly explained by the fact that eastward propagating waves (e.g., DE3) are ducted in the easterly background winds so that local angular frequency of tide becomes larger than the local Coriolis frequency [*Ekanayake et al.*, 1997; *Zhang et al.*, 2011]. The longitudinal dependency of ozone heating in the upper stratosphere might also be related. Further discussion is beyond the scope of this paper.

[38] The DW1 in the lower atmosphere was comprehensively examined. It was found that the characteristics are different between the tropics and the middle latitudes. The amplitude basically maximizes in the tropics, where the phase is constant as ∼18 LT within the troposphere and shows a downward progression from the stratosphere to the lower mesosphere. At middle latitudes, the amplitude maximizes in the upper stratosphere, while the phase is constant as ∼18 LT from the troposphere to the lower mesosphere. The DW1 shows intriguing seasonal variations from the tropical stratosphere to the lower mesosphere; the amplitude maximizes in January–February and in July–September, with an anti-symmetric structure being dominant.

[39] GSWM09 data were compared with SABER and reanalyses for the DW1. The basic features and seasonal variations found in SABER and reanalyses were reproduced reasonably well in GSWM09. However, the anti-symmetric structure in the tropics is too weak in GSWM. Also, the amplitude at middle latitudes in the upper stratosphere are considerably smaller than SABER and MERRA.

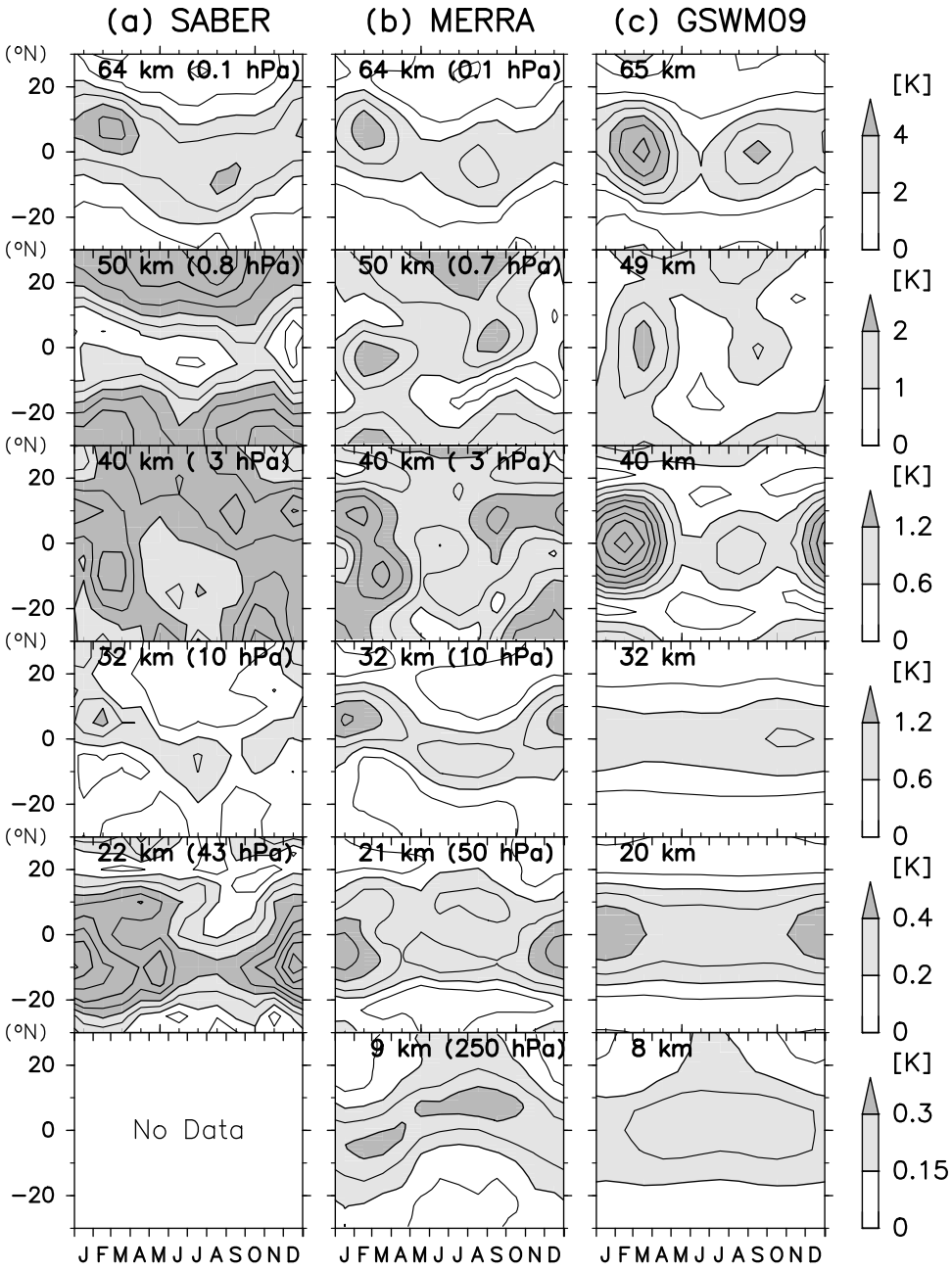


**Figure 11.** Tropical month–latitude distributions of amplitude for temperature DW1 approximately at 10, 20, 30, 40, 50 and 65 km. (a) SABER, (b) A-MERRA and (c) GSWM09. The actual altitude level is shown in each panel. Contour interval is 0.075 K, 0.1 K, 0.3 K, 0.3 K, 0.5 K and 1 K, for 10 km, 20 km, 30 km, 40 km, 50 km and 65 km, respectively. Color bar is shown on the right.

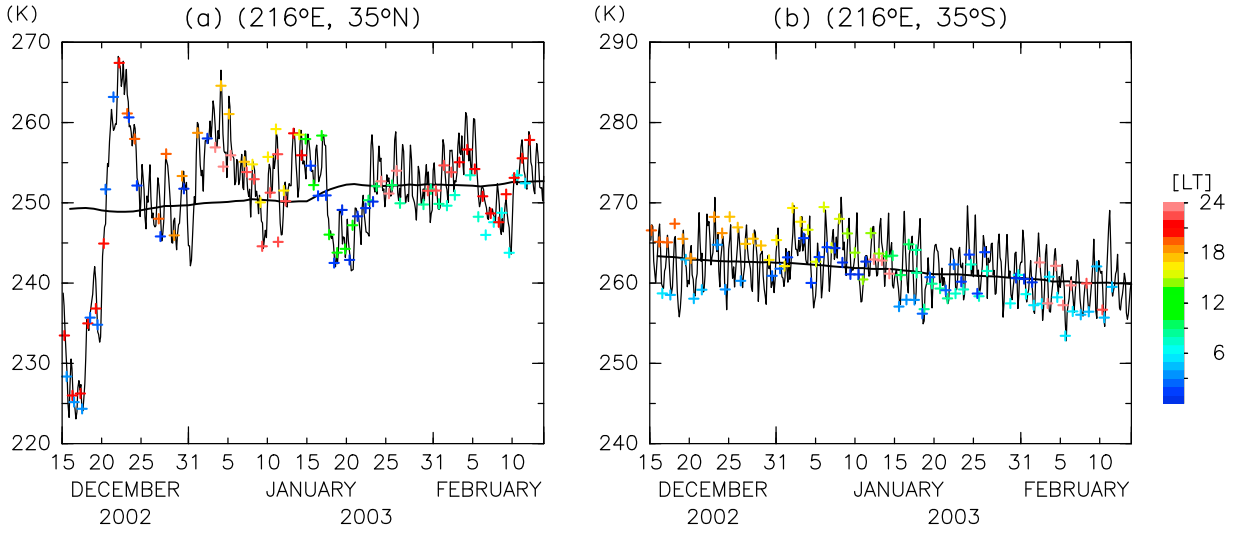


**Figure 12.** Time series of temperature at (a) (35°N, 216°E) and (b) (35°S, 216°E) at 50 km, as obtained by MERRA. Pluses are from MERRA sampled when SABER measurements are made with their color showing the measurement local time (see the color bar on the right-hand side); thick solid curves show the time series of 60-day running mean. Thin solid curves are the time series of MERRA data at original, 3-hourly time resolution.

[40] We mainly focused on the results from MERRA in this report. The difference in the diurnal tides among the reanalyses is relatively small, compared to that in the daily mean temperature. Nevertheless, ERA-Interim and CFSR reanalysis show the most similar results to those from SABER and MERRA. Vertical profiles from the tropical troposphere to the lower stratosphere in JRA25, NCEP1 and NCEP2 are different from those in MERRA. Also, the seasonal variations in the NCEP reanalyses are different from those in other data sets. Thus, we recommend the use of MERRA, ERA-Interim and CFSR for realistic tidal studies based on reanalyses, again with a caution that the amplitudes are small in the upper stratosphere to lower mesosphere.

[41] In our companion paper, the dynamical processes of observed DW1 will be investigated using MERRA reanalysis data, because the observed and modeled latitude-altitude structures are found to be captured by this data set.

## Appendix A: Comparison in the Daily Mean and Standard Deviation

[42] In this section, we briefly show the results of comparison in the daily mean and the standard deviation (STD) between SABER and reanalyses. SABER data at 83°S–83°N in 2002–2006 are used for analysis. For reanalyses, the data

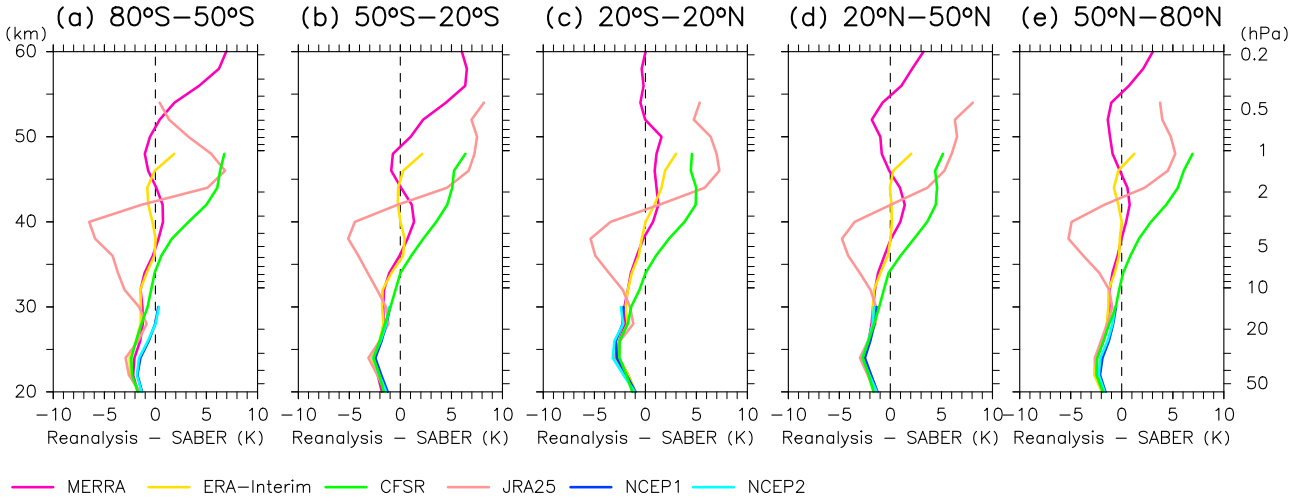


**Figure A1.** Vertical profiles of the difference in the daily mean temperature between reanalyses and SABER (Reanalysis minus SABER; S-DIF) for (a) 80°S–50°S, (b) 50°S–20°S, (c) 20°S–20°N, (d) 20°N–50°N, and (e) 50°N–80°N. The color allocation is the same as Figure 3.

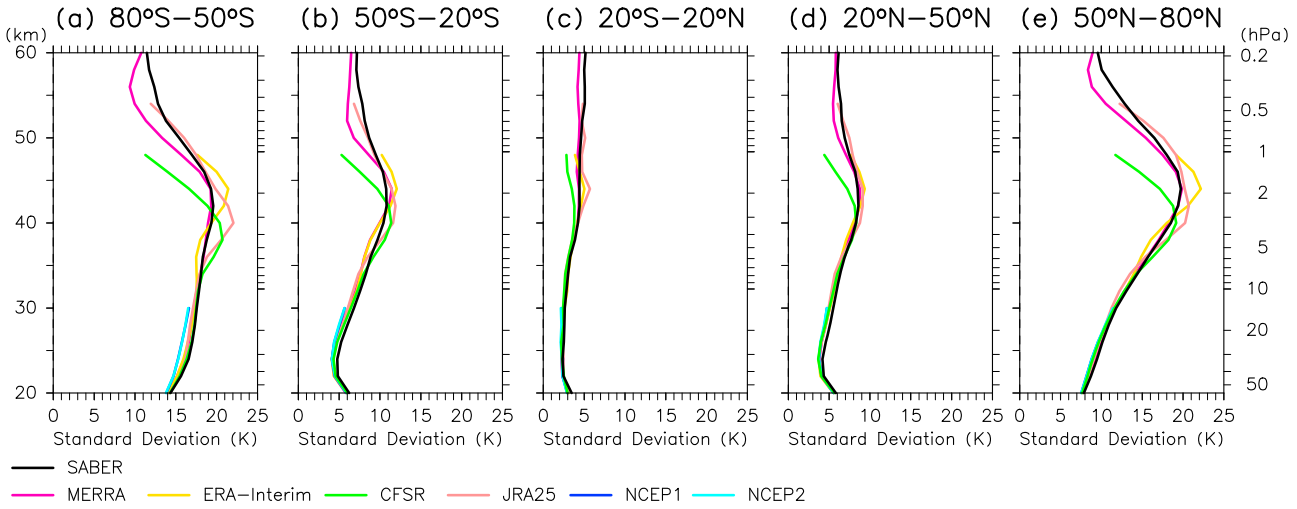


**Figure A2.** Same as Figure A1 but for the standard deviations. Black curves are for SABER.

at SABER measurement location/time are used for calculation (see section 3 for the method).

[43] Using these data, (1) the difference in the daily mean from the SABER (hereafter referred as S-DIF) and (2) the STD, are calculated. The S-DIF is defined as,

$$\frac{1}{n}\sum_{n}(T_R - T_S), \tag{A1}$$

where $n$ is total number of data, and $T_R$ and $T_S$ are temperatures from reanalyses and SABER, respectively. By definition, this quantity is regarded as the difference in daily zonal mean temperature. Note that *Remsberg et al.* [2008] reported that SABER Version 1.07 temperature data are too high by 1–3 K in the lower stratosphere (below ~40 km) but then too low by 1 K from the upper stratosphere to lower mesosphere (at 40–60 km), by comparing them with other satellite observation data, lidar data, and analysis data.

[44] Figure A1 shows vertical profiles of S-DIFs for 2002–2006 from six reanalyses averaged over different latitude regions: 80°S–50°S, 50°S–20°S, 20°S–20°N, 20°N–50°N and 50°N–80°N. Below 30 km, all reanalyses basically show S-DIFs of −3 K to −1 K except at ~20 km of 20°S–20°N. These negative S-DIFs are probably due to the positive bias in SABER of 1–3 K at these altitudes reported by *Remsberg et al.* [2008]; in other words, the bias in reanalysis temperatures (here, the bias means the deviation from the "true" value) can be ~ ±1 K in this altitude region. Above 30 km, S-DIFs are largely different among the data sets. Considering the positive bias of 1–3 K (the negative bias of 1 K) in SABER below 40 km (at 40–60 km) [*Remsberg et al.*, 2008], the MERRA performs best in reproducing the daily mean temperature in SABER. Considering the S-DIF and the bias in SABER, the bias in MERRA is estimated to be ~ ±1 K below 35 km, −3 to 1 K at 35–50 km and 4–5 K at ~60 km.

[45] Figure A2 shows vertical profiles of the STD for 2002–2006 from SABER and six reanalyses averaged over the five latitude regions. It is seen that the STD is largest (~15 K) in the stratosphere at mid-high latitudes, which would be largely caused by Rossby waves. We notice that the difference between SABER and reanalyses is small (~10%), compared to the difference in the diurnal component only (30–50% at the maximum; section 4.1).

## Appendix B: Sampling Issues due to Background Temperature Changes

[46] It is found that diurnal variations extracted from SABER measurement data suffer from sampling issues even after the 60-day running mean has been removed. In this section, we examine what kind of background temperature changes generates the spurious diurnal tides for SABER measurements (a similar discussion was made for MLS measurements by *Forbes and Wu* [2006]). Figure B1 shows the local time of SABER measurements at the equator and at 50°N in 2003. The discontinuity in each panel (e.g., 15 January) shows the occurrence of yaw maneuver. The change in measurement local time with longitude (orbit) is negligible during a day (<12 min). Also, the measurement local time on a given day of the year does not change considerably during the analysis period (e.g., the measurement time for ascending node at 50°N at the day 100 of 2002 (2006) is 1.1 LT (0.7 LT)). Thus, the following discussion is made for 2003.

[47] We consider a simple case where there are no diurnal variations. It is assumed that the background temperature changes in a form of

$$A\cos(\omega t - \alpha), \tag{B1}$$

where $A$ is amplitude, $\omega$ is time frequency, $t$ is time (day), and $\alpha$ is phase (rad). In the case that 60-day running mean has been removed for each $t$, the residual temperatures must satisfy the following condition for any $t$:

$$\int_{t-T_p/2}^{t+T_p/2} A\cos(\omega t - \alpha) = \frac{2A}{\omega}\cos(\omega t - \alpha)\sin\frac{\omega T_p}{2} = 0, \tag{B2}$$

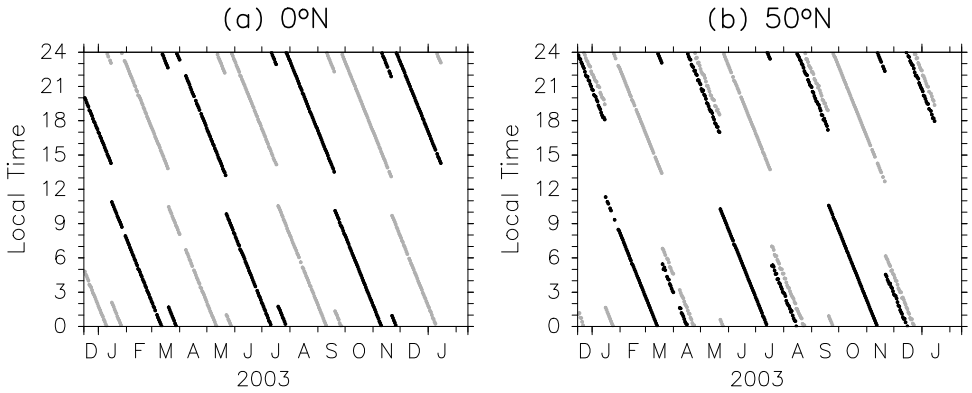


**Figure B1.** Time series of local-time for SABER measurements in 2003 at (a) the equator and (b) 50°N. Black and gray circles show ascending and descending nodes, respectively.

where $T_p$ = 60 (days). That is,

$$\omega = n\pi/T_p, \quad n = 2, 4, 6, \ldots$$
$$\Longleftrightarrow T_\omega = 120/n(\text{day}), \quad n = 2, 4, 6, \ldots, \tag{B3}$$

where $T_\omega = 2\pi/\omega$ (day) is time period. In other words, those waves satisfying equations of (B1) and (B3) can be contaminated into diurnal variations as observed using the present analysis method (section 2.1).

[48] Generally, when $A$ is given, the contamination depends on the following four factors: (1) latitude, (2) month, (3) frequency ($T_\omega$) and (4) phase ($\alpha$). Thus, the spurious diurnal component is calculated from 50°S to 50°N every 5°, for each month (the actual calculation is made using 60 day data; see section 3.2), for $T_\omega$ = 60, 30 and 15 (day), and for $\alpha = 0, \pi/4, \pi/2$ and $3\pi/4$, with $A$ = 1 (K). Since $A$ is constant, the results are regarded as the "efficiency" of contamination. Here, because we do not consider the "true" diurnal variations, the ascending and descending nodes are assumed to observe the same temperature for each day, but at different local times (e.g., Figure B1). Figure B2 shows an example of how the contamination occurs in the case of 50°N, January, $T_\omega$ = 60 and $\alpha$ = 0. In this case, it is found that the spurious diurnal component has an amplitude of ~80% of $A$. The spurious semidiurnal component also has a non-negligible amplitude, although the semidiurnal tides are not treated in the present study. Figure B3 shows the month–latitude distributions of the spurious diurnal amplitudes for the different values of $T_\omega$ and $\alpha$. Although the dependence on phase ($\alpha$) is somewhat complex, it can be said that higher latitude regions with longer wave periods are more sensitive to the sampling issues. The latitudinal dependency is caused by the fact that the difference of the measurement local time between ascending and descending nodes is close to 12 LT at lower latitude regions (Figure B1). Furthermore, the months when there are no yaw maneuvers (February, April, June, August, October and December; see Figure B1) have a smaller impact from the contamination.

[49] It is found in Figure B2 that the contamination is large in mid-to-high latitude regions of winter hemisphere stratosphere, with some longitudinal dependency. From the above discussion, in a particular month, the variability with $T_\omega$ = 30–60 (day) mainly results in the contamination, while the latitudinal dependency of the efficiency of contamination also plays a role. In fact, a spectral analysis on reanalysis data shows that the components with $T_\omega$ = 30–60 (day) have large amplitudes in the region where large contamination are observed in Figure 1 (not shown). In addition, those components have amplitudes of 4–7 K at 40–50°N at 40–50 km in January (cf. Figure A2); the spurious diurnal amplitudes are estimated from Figure B3 to be ~5 K. This is roughly

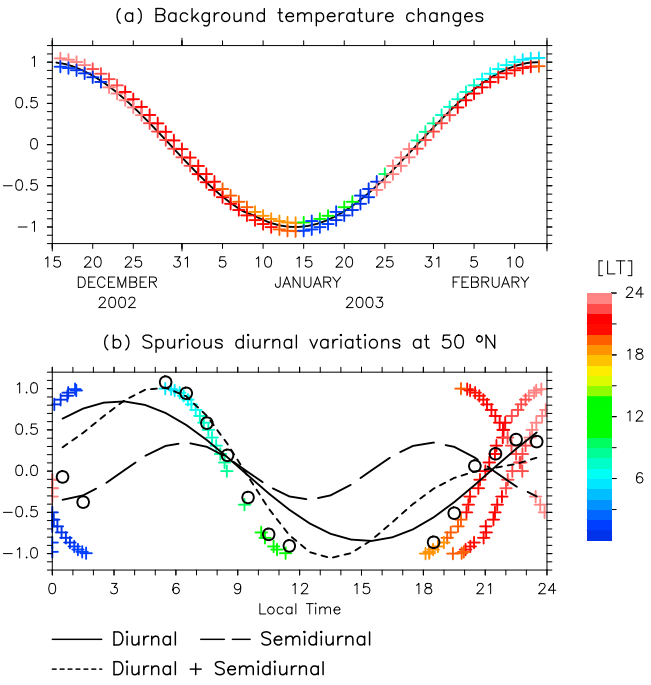


**Figure B2.** (a) Background temperature changes with $A$ = 1, $T_\omega$ = 60 (day) and $\alpha$ = 0 in equation (A1). Pluses represents the SABER sampling with their color showing the local time of measurements at 50°N in January (see the color bar on the right hand side). (b) Observed temperature sorted in local-time. Open circles show the composite temperature in the hourly bins. Solid and dashed curves show the diurnal and semidiurnal components, respectively, as extracted with the least square fitting. Dotted curve shows the diurnal variations with the diurnal and semidiurnal components only.

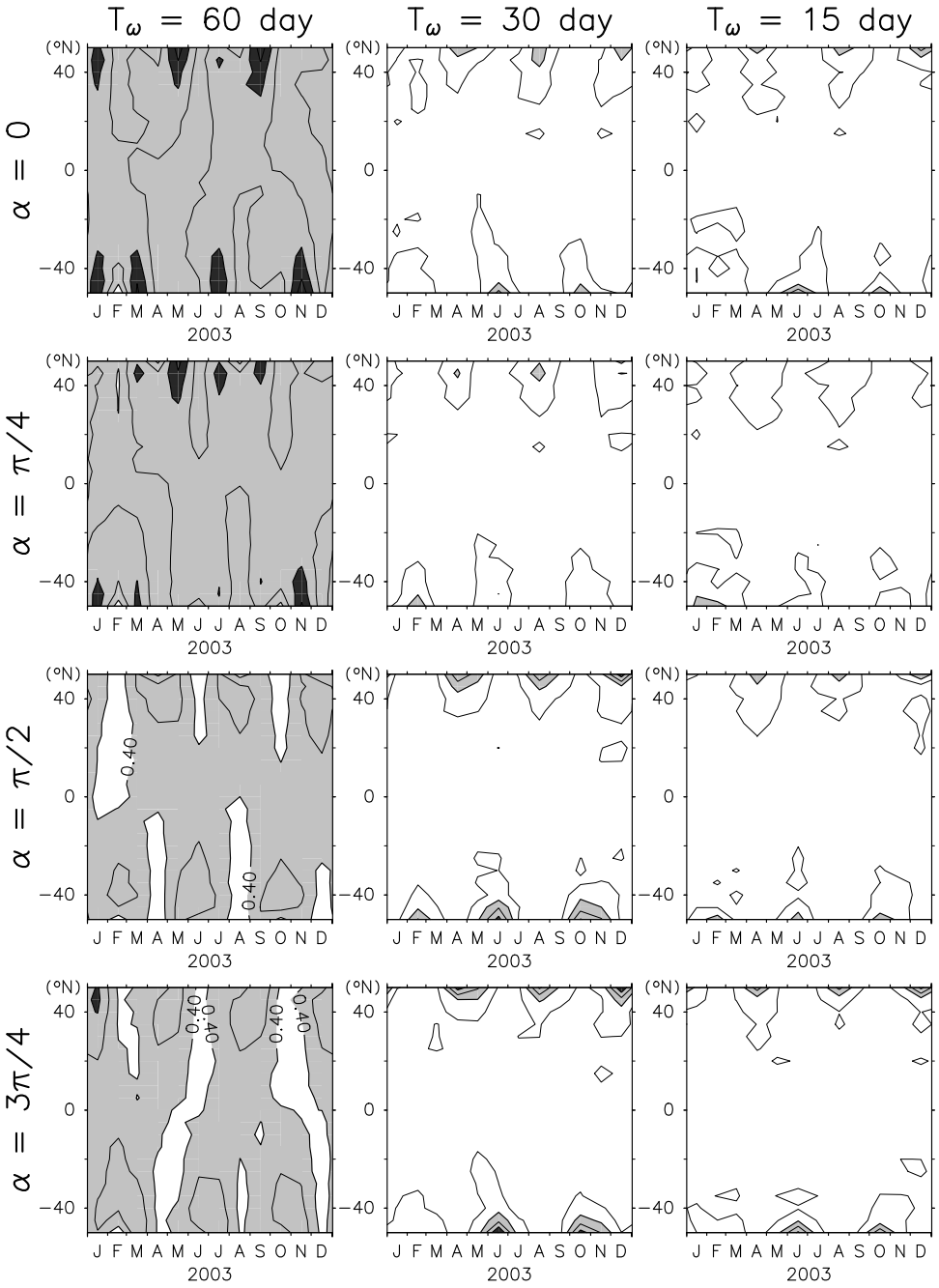


**Figure B3.** Month–latitude distributions of the spurious diurnal component due to background temperature changes in 2003, as observed by SABER measurements in the case of $A$ = 1 (K). $T_\omega$ = (left) 60, (middle) 30 and (right) 15 (day); $\alpha$ = 0 (first row), $\pi/4$ (second row), $\pi/2$ (third row) and $3\pi/4$ (fourth row). Contour interval is 0.2 K. The regions with >0.8 K (>0.4 K) colored dark (light) gray. See text for details.

consistent with the spurious diurnal amplitudes of 5–8 K as observed in Figure 1.

[50] **Acknowledgments.** NCEP1 and NCEP2 data were provided by the NOAA/OAR/ESRL PSD. ERA-Interim data were provided by the ECMWF through their Web site. JRA25/JCDAS data were provided by the JMA and CRIEPI. MERRA data were provided by NASA/GSFC/GMAO. CFSR data were provided through NOAA/NCDC. This study was supported in part by Global COE Program (Establishment of Center for Integrated Field Environmental Science), the Ministry of Education, Culture, Sports, Science and Technology (MEXT), Japan. The first author was supported in part by the MEXT through Grants-in-Aid for JSPS Fellows (22002958). Part of this study was made while the first author stayed at NCAR/HAO. X. Zhang and J.M. Forbes were supported under ATM grant award ATM-0903179 from the National Science to the University of Colorado. We thank Nicholas Pedatella and three anonymous reviewers for valuable comments on the original manuscript. We also thank Kazutoshi Onogi and Wesley Ebisuzaki for providing information about the satellite data assimilation in JRA25 and NCEPs, respectively. The first author is grateful to Anne Smith, Julio Bacmeister, Steven Pawson, Masato Shiotani, Makoto Suzuki, and Hironori Umezu for fruitful discussions and comments. All figures were produced using the GFD-DENNOU Library. The National Center for Atmospheric Research is sponsored by the National Science Foundation.

## References

Alexander, S. P., and T. Tsuda (2008), Observations of the diurnal tide during seven intensive radiosonde campaigns in Australia and Indonesia, *J. Geophys. Res.*, *113*, D04109, doi:10.1029/2007JD008717.

Bloom, S., L. Takacs, A. DaSilva, and D. Ledvina (1996), Data assimilation using incremental analysis updates, *Mon. Weather Rev.*, *124*, 1256–1271.

Chang, L., S. Palo, M. Hagan, J. Richter, R. Garcia, D. Riggin, and D. Fritts (2008) Structure of the migrating diurnal tide in the Whole Atmosphere Community Climate Model (WACCM), *Adv. Space Res.*, *41*, 1398–1407.

Chapman, S., and R. S. Lindzen (1970), *Atmospheric Tides*, 200 pp., D. Reidel, New York.

Courtier, P., J.-N. Thepaut, and A. Hollingsworth (1994), A strategy for operational implementation of 4D-Var, using and incremental approach, *Q. J. R. Meteorol. Soc.*, *120*, 1367–1388.

Dai, A., and J. Wang (1999), Diurnal and semidiurnal tides in global surface pressure fields, *J. Atmos. Sci.*, *56*, 3874–3891.

Dee, D. P., et al. (2011), The ERA-Interim reanalysis: configuration and performance of the data assimilation system, *Q. J. R. Meteorol. Soc.*, *137*, 553–597.

Ekanayake, E. M. P., T. Aso, and S. Miyahara (1997), Background wind effect on propagation of nonmigrating diurnal tides in the middle atmosphere, *J. Atmos. Terr. Phys.*, *59*, 401–429.

Forbes, J. M., and D. Wu (2006), Solar tides as revealed by measurements of mesosphere temperature by the MLS experiment on UARS, *J. Atmos. Sci.*, *63*, 1776–1797.

Forbes, J. M., M. Kilpatrick, D. Fritts, A. H. Manson, and R. A. Vincent (1997), Zonal mean and tidal dynamics from space: An empirical examination of aliasing and sampling issues, *Ann. Geophys.*, *15*, 1158–1164.

Forbes, J. M., J. Russell, S. Miyahara, X. Zhang, S. Palo, M. Mlynczak, C. J. Mertins, and M. E. Hagan (2006), Troposphere-thermosphere tidal coupling as measured by the SABER instrument on TIMED during July–September 2002, *J. Geophys. Res.*, *111*, A10S06, doi:10.1029/2005JA011492.

Forbes, J. M., X. Zhang, S. Palo, J. Russell, C. J. Mertens, and M. Mlynczak (2008), Tidal variability in the ionospheric dynamo region, *J. Geophys. Res.*, *113*, A02310, doi:10.1029/2007JA012737.

Hagan, M. E., J. M. Forbes, and F. Vial (1995), On modeling migrating solar tides, *Geophys. Res. Lett.*, *22*, 893–896.

Hagan, M. E., M. D. Burrage, J. M. Forbes, J. Hackney, W. J. Randel, and X. Zhang (1999), GSWM-98: Results for migrating solar tides, *J. Geophys. Res.*, *104*(A4), 6813–6827.

Haurwitz, B., and A. D. Cowley (1973), The diurnal and semidiurnal barometric oscillations, global distribution and annual variation, *Pure Appl. Geophys.*, *102*, 193–222.

Hitchman, M., and C. B. Leovy (1985), Diurnal tide in the equatorial middle atmosphere as seen in LIMS temperatures, *J. Atmos. Sci.*, *42*, 557–561.

Huang, F. T., H. G. Mayr, C. A. Reber, T. Killeen, J. Russell, M. Mlynczak, W. Skinner, and J. Mengel (2006), Diurnal variations of temperature and winds inferred from TIMED and UARS measurements, *J. Geophys. Res.*, *111*, A10S04, doi:10.1029/2005JA011426.

Huang, F. T., R. D. McPeters, P. K. Bhartia, H. G. Mayr, S. M. Frith, J. M. Russell III, and M. G. Mlynczak (2010), Temperature diurnal variations (migrating tides) in the stratosphere and lower mesosphere based on measurements from SABER on TIMED, *J. Geophys. Res.*, *115*, D16121, doi:10.1029/2009JD013698.

Japanese Meteorological Agency (2002), Outline of the operational numerical weather prediction at the Japan Meteorological Agency: Appendix to WMO Numerical Weather Prediction Progress Report, report, 158 pp., World Meteorol. Org., Geneva, Switzerland.

Kalnay, E., et al. (1996), The NCEP/NCAR 40-year reanalysis project, *Bull. Am. Meteorol. Soc.*, *77*, 437–471.

Kanamitsu, M., W. Ebisuzaki, J. Woollen, S.-K. Yang, J. J. Hnilo, M. Fiorino, and G. L. Potter (2002), NCEP-DEO AMIP-II reanalysis (R-2), *Bull. Am. Meteorol. Soc.*, *83*, 1631–1643.

Lieberman, R. S. (1991), Nonmigrating diurnal tides in the equatorial middle atmosphere, *J. Atmos. Sci.*, *48*, 1112–1123.

Liu, H.-L., T. Li, C.-Y. She, J. Oberheide, Q. Wu, M. E. Hagan, J. Xu, R. G. Roble, M. G. Mlynczak, and J. Russell III (2007), Comparative study of short-term diurnal tidal variability, *J. Geophys. Res.*, *112*, D18108, doi:10.1029/2007JD008542.

Lu, X., A. Z. Liu, J. Oberheide, Q. Wu, T. Li, Z. Li, G. R. Swenson, and S. J. Franke (2011), Seasonal variability of the diurnal tide in the mesosphere and lower thermosphere over Maui, Hawaii (20.7°N, 156.3°W), *J. Geophys. Res.*, *116*, D17103, doi:10.1029/2011JD015599.

Mclandress, C. (1997), Seasonal variability of the diurnal tide: Results from the Canadian middle atmosphere general circulation model, *J. Geophys. Res.*, *102*(D25), 29,747–29,764.

Mukhtarov, P., D. Pancheva, and B. Andonov (2009), Global structure and seasonal and interannual variability of the migrating diurnal tide seen in the SABER/TIMED temperatures between 20 and 120 km, *J. Geophys. Res.*, *114*, A02309, doi:10.1029/2008JA013759.

Onogi, K., et al. (2007), The JRA-25 reanalysis, *J. Meteorol. Soc. Jpn.*, *85*, 369–432.

Parrish, D. F., and J. C. Derber (1992), The National Meteorological Center's spectral statistical interpolation analysis system, *Mon. Weather Rev.*, *120*, 1747–1763.

Pirscher, B., U. Foelsche, M. Borsche, G. Kirchengast, and Y.-H. Kuo (2010), Analysis of migrating diurnal tides detected in FORMOSAT-3/COSMIC temperature data, *J. Geophys. Res.*, *115*, D14108, doi:10.1029/2009JD013008.

Ray, R. D. (2001), Comparison of global analyses and station observations of the $S_2$ barometric tide, *J. Atmos. Terr. Phys.*, *63*, 1085–1097.

Ray, R. D., and R. M. Ponte (2003), Barometric tides from ECMWF operational analyses, *Ann. Geophys.*, *21*, 1897–1910.

Reed, R. J., M. J. Oard, and M. Sieminski (1969), A comparison of observed and theoretical diurnal tidal motions between 30 and 60 kilometers, *Mon. Weather Rev.*, *97*, 456–459.

Remsberg, E. E., et al. (2008), Assessment of the quality of the Version 1.07 temperature-versus-pressure profiles of the middle atmosphere from TIMED/SABER, *J. Geophys. Res.*, *113*, D17101, doi:10.1029/2008JD010013.

Rienecker, M. M., et al. (2011), MERRA: NASA' s Modern-Era Retrospective analysis for Research and Applications, *J. Clim.*, *24*, 3624–3648.

Riggin, D. M., E. Kudeki, Z. Feng, M. F. Sarango, and R. S. Lieberman (2002), Jicamarca radar observations of the diurnal and semidiurnal tide in the troposphere and lower stratosphere, *J. Geophys. Res.*, *107*(D8), 4062, doi:10.1029/2001JD001216.

Saha, S., et al. (2010), The NCEP climate forecast system reanalysis, *Bull. Am. Meteorol. Soc.*, *91*, 1015–1057.

Sakazaki, T., M. Fujiawra, and H. Hashiguchi (2010), Diurnal variations of upper tropospheric and lower stratospheric winds over Japan as revealed with middle and upper atmosphere radar (34.85°N, 136.10°E) and five reanalysis data sets, *J. Geophys. Res.*, *115*, D24104, doi:10.1029/2010JD014550.

Swinbank, R., R. L. Orris, and D. L. Wu (1999), Stratospheric tides and data assimilation, *J. Geophys. Res.*, *104*(D14), 16,929–16,941.

Tokioka, T., and I. Yagai (1987), Atmospheric tides appearing in a global circulation model, *J. Meteorol. Soc. Jpn.*, *65*, 423–437.

Tsuda, T., Y. Murayama, H. Wiryosumarto, S. W. B. Harijono, and S. Kato (1994), Radiosonde observations of equatorial atmosphere dynamics over Indonesia: 1. Equatorial waves and diurnal tides, *J. Geophys. Res.*, *99*(D5), 10,491–10,505.

van den Dool, H. M., S. Saha, J. Schemm, and J. Huang (1997), A temporal interpolation method to obtain hourly atmospheric surface pressure tides in reanalyses 1979–1995, *J. Geophys. Res.*, *102*, 22,013–22,024.

Vincent, R. A., T. Tsuda, and S. Kato (1988), A comparative study of mesospheric solar tides observed at Adelaide and Kyoto, *J. Geophys. Res.*, *93*(D1), 699–708.

Wallace, J. M., and F. R. Hartranft (1969), Diurnal wind variations, surface to 30 kilometers, *Mon. Weather Rev.*, *97*, 446–455.

Wallace, J. M., and R. F. Tadd (1974), Some further results concerning the vertical structure of atmospheric tidal motions within the lowest 30 kilometers, *Mon. Weather Rev.*, *102*, 795–803.

Ward, W. E., J. Oberheide, M. Riese, P. Preusse and D. Offermann (1999), Tidal signatures in temperature data from CRISTA 1 mission, *J. Geophys. Res.*, *104*, 16,391–16,403.

Ward, W. E., et al. (2010), On the consistency of model, ground-based, and satellite observations of tidal signatures: Initial results from the CAWSES tidal campaigns, *J. Geophys. Res.*, *115*, D07107, doi:10.1029/2009JD012593.

Williams, C. R., and S. K. Avery (1996a), Diurnal nonmigrating tidal oscillations forced by deep convective clouds, *J. Geophys. Res.*, *101*(D2), 4079–4091.

Williams, C. R., and S. K. Avery (1996b), Diurnal winds observed in the tropical tropopause using 50 MHz wind profilers, *J. Geophys. Res.*, *101*(D10), 15,051–15,060.

Wu, D. L., C. McLandress, W. G. Read, J. W. Waters and L. Froidevaux (1998), Equatorial diurnal variations observed in UARS Microwave Limb Sounder temperature during 1991–1994 and simulated by the Canadian Middle Atmosphere Model, *J. Geophys. Res.*, *103*, 8909–8917.

Wu, Q., D. A. Ortland, T. L. Killeen, R. G. Roble, M. E. Hagan, H.-L. Liu, S. C. Solomon, J. Xu, W. R. Skinner, and R. J. Niciejewski (2008), Global distribution and interannual variations of mesospheric and lower thermospheric neutral wind diurnal tide: 1. Migrating tide, *J. Geophys. Res.*, *113*, A05308, doi:10.1029/2007JA012542.

Wu, W.-S., R. J. Purser, and D. F. Parrish (2002), Three-dimensional variational analysis with spatially inhomogeneous covariances, *Mon. Weather Rev.*, *130*, 2905–2916.

Xie, F., D. L. Wu, C. O. Ao, and A. J. Mannucci (2010), Atmospheric diurnal variations observed with GPS radio occulation soundings, *Atmos. Chem. Phys.*, *10*, 6889–6899.

Xu, J., A. K. Smith, W. Yuan, H.-L. Liu, Q. Wu, M. G. Mlynczak, and J. M. Russell III (2007), Global structure and long-term variations of zonal mean temperature observed by TIMED/SABER, *J. Geophys. Res.*, *112*, D24106, doi:10.1029/2007JD008546.

Xu, J., A. K. Smith, H.-L. Liu, W. Yuan, Q. Wu, G. Jiang, M. G. Mlynczak, J. M. Russell III, and S. J. Franke (2009), Seasonal and quasi-biennial variations in the migrating diurnal tide observed by Thermosphere, Ionosphere, Mesosphere, Energetics and Dynamics (TIMED), *J. Geophys. Res.*, *114*, D13107, doi:10.1029/2008JD011298.

Zeng, Z., W. Randel, S. Sokolovskiy, C. Deser, Y.-H. Kuo, M. Hagan, J. Du, and W. Ward (2008), Detection of migrating diurnal tide in the tropical upper troposphere and lower stratosphere using the Challenging Minisatellite Payload radio occultation data, *J. Geophys. Res.*, *113*, D03102, doi:10.1029/2007JD008725.

Zhang, X., J. M. Forbes, M. E. Hagan, J. M. Russell III, S. E. Palo, C. J. Mertens, and M. G. Mlynczak (2006), Monthly tidal temperatures 20–120 km from TIMED/SABER, *J. Geophys. Res.*, *111*, A10S08, doi:10.1029/2005JA011504.

Zhang, X., J. M. Forbes, and M. E. Hagan (2010a), Longitudinal variation of tides in the MLT region: 1. Tides driven by tropospheric net radiative heating, *J. Geophys. Res.*, *115*, A06316, doi:10.1029/2009JA014897.

Zhang, X., J. M. Forbes, and M. E. Hagan (2010b), Longitudinal variation of tides in the MLT region: 2. Relative effects of solar radiative and latent heating, *J. Geophys. Res.*, *115*, A06317, doi:10.1029/2009JA014898.

Zhang, X., J. M. Forbes, and M. E. Hagan (2011), Seasonal-latitudinal variation of the eastward-propagating diurnal tide with zonal wavenumber 3 in the MLT: Influences of heating and background wind distribution, *J. Atmos. Terr. Phys.*, *78–79*, 37–43, doi:10.1016/j.jastp.2011.03.005.